Supporting Information

Synthesis and Structure of a Family of Rhodium Polystannide Clusters $[Rh@Sn_{10}]^{3-}$, $[Rh@Sn_{12}]^{3-}$, $[Rh_2@Sn_{17}]^{6-}$ and the First Tri-Fused Stannide, $[Rh_3@Sn_{24}]^{5-}$

Chao Liu, Xiao Jin, Lei-Jiao Li, Jun Xu, John E. McGrady,* and Zhong-Ming Sun*

Abstract: Through relatively subtle changes in reaction conditions, we have been able to isolate four distinct Rh/Sn cluster compounds, $[Rh@Sn_{10}]^{3-}$ and $[Rh@Sn_{12}]^{3-}$, $[Rh_2@Sn_{17}]^{6-}$ and $[Rh_3@Sn_{24}]^{5-}$, from the reaction of K_4Sn_9 with $[(COE)_2Rh(\mu\text{-}Cl)]_2$(COE= cyclooctene). The last of these has a hitherto unknown molecular topology, an edge-fused polyhedron containing three $Rh@Sn_{10}$ subunits, and represents the largest endohedral Group 14 Zintl cluster yet to have been isolated from solution. DFT has been used to place these new species in the context of known cluster chemistry, and their structural properties provide clear evidence that the 4*d* orbitals of Rh are far from inert. ESI-MS experiments on the reaction mixtures reveal the ubiquitous presence of $\{RhSn_8\}$ fragments that may play a role in cluster growth.

DOI: 10.1002/anie.2016XXXXX

Table of Contents

1. Experimental Procedures

All manipulations and reactions were performed in a nitrogen atmosphere using standard Schlenk or glovebox techniques. En (Aldrich, 99%) and DMF (Aldrich, 99.8%) were freshly distilled by CaH_2 prior to use. Tol (Aldrich, 99.8%) was distilled from sodium/benzophenone under nitrogen and stored under nitrogen. 2,2,2-crypt (4,7,13,16,21,24-Hexaoxa-1,10-diazabicyclo (8.8.8) hexacosane, purchased from Sigma-Aldirich, 98%) was dried in vacuum for one day prior to use. K_4Sn_9 was synthesized by heating the elements K and Sn (K (Aldrich, 99%), Sn (Aldrich, 99.8%)) at 1000℃ for two days in a niobium tube. $[(COE)_2Rh(u\text{-}Cl)]_2$ was prepared according to literature methodology.[1]

X-ray Diffraction. Suitable single crystals were selected for X-ray diffraction analyses. Crystallographic data were collected on a Bruker Apex II CCD diffractometer with graphite-monochromated Mo Kα radiation (λ = 0.71073 Å). Data processing was accomplished with the SAINT program. Structures were solved using direct methods and then refined using SHELXL-2014 [2] to convergence, in which all the non-hydrogen atoms were refined anisotropically during the final cycles. All hydrogen atoms of the organic molecule were placed by geometrical considerations and were added to the structure factor calculation. Positional disorder was found in the cluster site in compound **1**, and this was modeled accordingly (see the Supporting Information for details). Non-merohedral twinning in the crystal **1** was identified [Twin Rot Mat within PLATON (Spek, 2009)],[3] and the crystal was refined with hkl 5 format. The twin law gives a final refined BASF parameter of 0.234(3). In **3**, one en molecule was refined at split positions with partial occupations. A summary of the crystallographic data for these two complexes is listed in Table S1. A summary of the crystallographic data for these complexes is listed in Table S1, and selected bond distances are given in Tables S2-S6. CCDC entries are 1847077-1847079 for compounds **1**, **2a** and **3**, 1847080 for compound **2b** and 1811035 for compound **4** contain the supplementary crystallographic data for this paper.

Electrospray Ionization Mass Spectrometry (ESI-MS) Investigations. Negative ion mode ESI-MS of the en reaction mixture were measured on an Agilent Technologies ESI-TOF-MS (6224). ESI-MS of the DMF reaction mixture and ESI-MS of the single crystal of $[Rh@Sn_{10}]^{3-}$, $[Rh@Sn_{10}]^{3-}$ and $[Rh_2@Sn_{17}]^{6-}$ were performed on an LTQ linear ion trap spectrometer. The spray voltage was 5.48 kV and the capillary temperature was keep at 300℃. The capillary voltage was 30 V. The samples were made up inside a glovebox under an inert atmosphere and rapidly transferred to the spectrometer in an air-tight syringe by direct infusion with a Harvard syringe pump at 15 uL/ min.

^{119}Sn Liquid NMR Investigations： All NMR samples were prepared in a nitrogen atmosphere. Solutions for NMR measurements were prepared by dissolving single crystals of $[K(2,2,2\text{-crypt})]_3[Rh@Sn_{10}]$•en (**1**) and $[K(2,2,2\text{-crypt})]_3[Rh@Sn_{12}]$•2Tol (**2a**) in en. The ^{119}Sn liquid NMR spectra were recorded on a Bruker Avance IIIHD spectrometer with an observed frequency of 149 MHz (^{119}Sn) at 20°C. One pulse NMR experiments were performed with a short flip angle of 30° and a long recycle delay of 60 s. The ^{119}Sn chemical shifts were referenced to SnO_2 as ans external standard, which is −604.3 ppm relative to $(CH_3)_4Sn$.

Energy Dispersive X-ray (EDX) Spectroscopy. EDX Analysis was performed using a scanning electron microscope (Hitachi S-4800) equipped with a Bruker AXS XFlash detector 4010. Data acquisition was performed with an acceleration voltage of 20 kV and an accumulation time of 150 s.

Methods of the Quantum Chemical Investigations. Density functional theory calculations were performed using the Amsterdam Density Functional package (ADF2017.01) [4-6] using the gradient-corrected (GGA) functional proposed by Becke and Perdew (BP86) [7, 8]. A Slater-type basis sets of triple-ζ quality, extended with a single polarisation function (TZP), was used to describe Co/Ni/Rh while a DZP basis set was used to describe Sn.[9] Core orbitals up to 2*p* (Co/Ni), 3*d* (Rh) and 4*p* (Sn) were frozen. Relativistic corrections were incorporated using the Zero Order Relativistic Approximation (ZORA).[10] All structures were optimized using the gradient algorithm of Versluis and Ziegler.[11] The effect of surrounding cations was modelled using a continuum solvation model (the Conductor-like Screening Model, COSMO) with ε = 78.39.[12] Frequencies were computed analytically.

Synthesis of $[K(2,2,2\text{-crypt})]_3[Rh@Sn_{10}]$•en (1) and $[K(2,2,2\text{-crypt})]_3[Rh@Sn_{12}]$•2Tol (2a): K_4Sn_9 (122 mg, 0.10 mmol) was weighed into a 10 mL vial inside a glovebox and dissolved in en (3 mL). After stirring for two hours, the dark red solution was filtered onto a mixture of $[(COE)_2Rh(u\text{-}Cl)]_2$ (49.7mg, 0.10mmol) and 2,2,2-crypt (151 mg, 0.4 mmol) and allowed to stir for a further two hours. The resulting dark brown solution was filtered through glass wool and transferred to a test tube, then carefully layered by toluene (5 mL) to allow for crystallization. Large black plate-like crystals of $[K(2,2,2\text{-crypt})]_3[Rh@Sn_{10}]$•2en (**1a**), together with a few rod-like crystals of $[K(2,2,2\text{-crypt})]_3[Rh@Sn_{12}]$•2Tol (**2a**), were isolated after two weeks in approximately 40% yield in total (based on precursor K_4Sn_9 used). The two products could be distinguished visually and separated mechanically.

Synthesis of $\{K_3[K(2,2,2\text{-crypt})]_3[Rh_2@Sn_{17}]\}$•4en (3): The synthesis of **3** followed exactly the same initial protocol described above for **1** and **2a**. After removing the crystals of **1** and **2a**, the solution was triturated with toluene and filtered through tightly packed glass wool in a pipet. Small quantities of dark brown thin plate-shaped of $\{K_3[K(2,2,2\text{-crypt})]_3[Rh_2@Sn_{17}]\}$•4en **(3)** crystallized at the wall of the tube after an additional two weeks in approximately 10% yield with regard to K_4Sn_9.

Synthesis of $[K(2,2,2\text{-crypt})]_5[Rh_3@Sn_{24}]$•2DMF•Tol (4):

Method **1**: K_4Sn_9 (122 mg, 0.10 mmol) was weighed into a 10 mL vial inside a glovebox and dissolved in en (3 mL). After stirring for an hour, the dark red solution was filtered onto a mixture of $[(COE)_2Rh(u\text{-}Cl)]_2$ (49.7mg, 0.10mmol) and 2,2,2-crypt (151 mg, 0.4 mmol) and allowed to stir for two hours. After removal of the en solvent, the solid residue was redissolved in DMF and heated at 50 °C for six hours. The mixture is allowed to cool to room temperature for another 30 minutes. The dark green solution was filtered through glass wool and transferred to a test tube, then carefully layered by toluene to allow for crystallization. Small quantities of plate-like crystals of **4** and brown rod-like crystals of $[K(2,2,2\text{-crypt})]_3[Rh@Sn_{12}]$•2DMF (**2b**) were isolated after four weeks. The yield is ~25% in total based on K_4Sn_9.

Method **2** : $[K(2,2,2\text{-crypt})]_3[Rh@Sn_{10}]$•en (150 mg, 0.06 mmol) was weighed into a 10 mL vial inside a glovebox and dissolved in DMF (2 mL). The resulting solution was heated at 50 °C for 6 hours. The mixture is allowed to cool to room temperature for another 30 min, then was filtered through glass wool and layered by toluene to allow for crystallization. Black plate-like crystals of $[K(2,2,2\text{-crypt})]_5[Rh_3@Sn_{24}]$•2DMF•Tol were isolated after four weeks (30% yield based on **1**).

2. Crystallographic Supplementation

Table S1. X-ray measurements and structure solution of the compounds.

Compound	**1**	**2a**	**3**	**4**	**2b**
Empirical formula	$C_{56}H_{116}K_3N_8O_{18}RhSn_{10}$	$C_{25}H_{44}O_6N_2KRh_{0.33}Sn_4$	$C_{62}H_{140}N_{14}O_{18}K_6Rh_2Sn_{17}$	$C_{103}H_{202}N_{12}O_{32}K_5Rh_3Sn_{24}$	$C_{30}H_{61}N_4O_{10}K_{1.5}Rh_{0.5}Sn_6$
Fw (g mol^{-1})	2595.68	1016.78	3828.32	5473.54	1458.05
Crystal system	triclinic	trigonal	monoclinic	triclinic	monoclinic
Space group	P-1	R-3	$P2_1/n$	P-1	C2/c
a/Å	15.142(3)	24.749(3)	21.5558(14)	16.3305(8)	27.304(5)
b/Å	15.879(4)	24.749(3)	16.1668(10)	19.4097(19)	17.505(3)
c/Å	19.180(5)	29.868(3)	33.205(2)	28.6354(15)	21.668(4)
α/ º	81.348(5)	90	90	94.7860(10)	90
β/º	87.147(4)	90	97.8280(10)	98.7350(10)	97.132(4)
γ/º	74.041(5)	120	90	112.5900(10)	90
V/ Å^3	4383.2(17)	15843(4)	11463.6(12)	8181.8(7)	10274(3)
Z	2	18	4	2	8
F(000)	2510.0	8820.0	7224.0	5180	5600
2Θ range for data collection/°	2.696 to 50.136	3.292 to 52.14	3.16 to 52.162	2.79 to 52.212	3.006 to 52.108
Reflections collected/ unique	15012/ 15012	6968/0/348	22635/85/1091	51523/32183	31375/10093
ρcalcd (g cm^{-3})	1.968	1.918	2.219	2.222	1.888
μ (Mo Kα)/ mm^{-1}	3.180	3.110	4.181	4.069	3.194
R1/wR_2(I>2σ(I))	0.0707/ 0.1831	0.0427/ 0.0929	0.0315/ 0.0693	0.0515/ 0.1114	0.0477/0.1150
R1, wR_2 (all data)	0.1032/ 0.2052	0.0636/0.1060	0.0410/ 0.0737	0.1018/ 0.1352	0.0711/0.1254
GooF (all data)	1.043	1.053	1.011	1.013	1.057
Data completeness	97%	100%	100%	99%	100%
Max.peak/hole /e–·Å^{-3}	2.13/-1.86	2.73/-1.11	2.87/-1.71	2.47/-1.65	2.30/-1.24

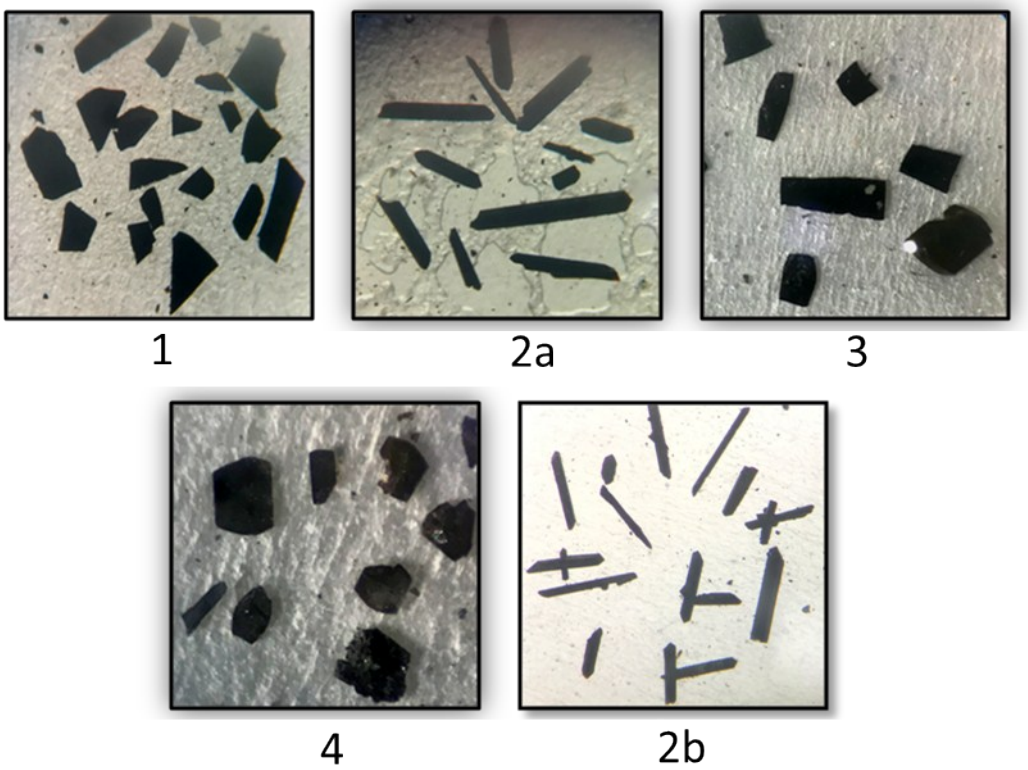

Figure 1. (a) Black large plate-shaped crystals of **1**. (b) Brown rod-like crystals of **2a**. (c) Dark brown thin plate-shaped crystals of **3**. (d) Black plate -type single crystal of **4**. (e) Brown rod-like crystals of **2b**.

2.1 Structure of $[K(2,2,2\text{-crypt})]_3[Rh@Sn_{10}]\bullet en$ (1)

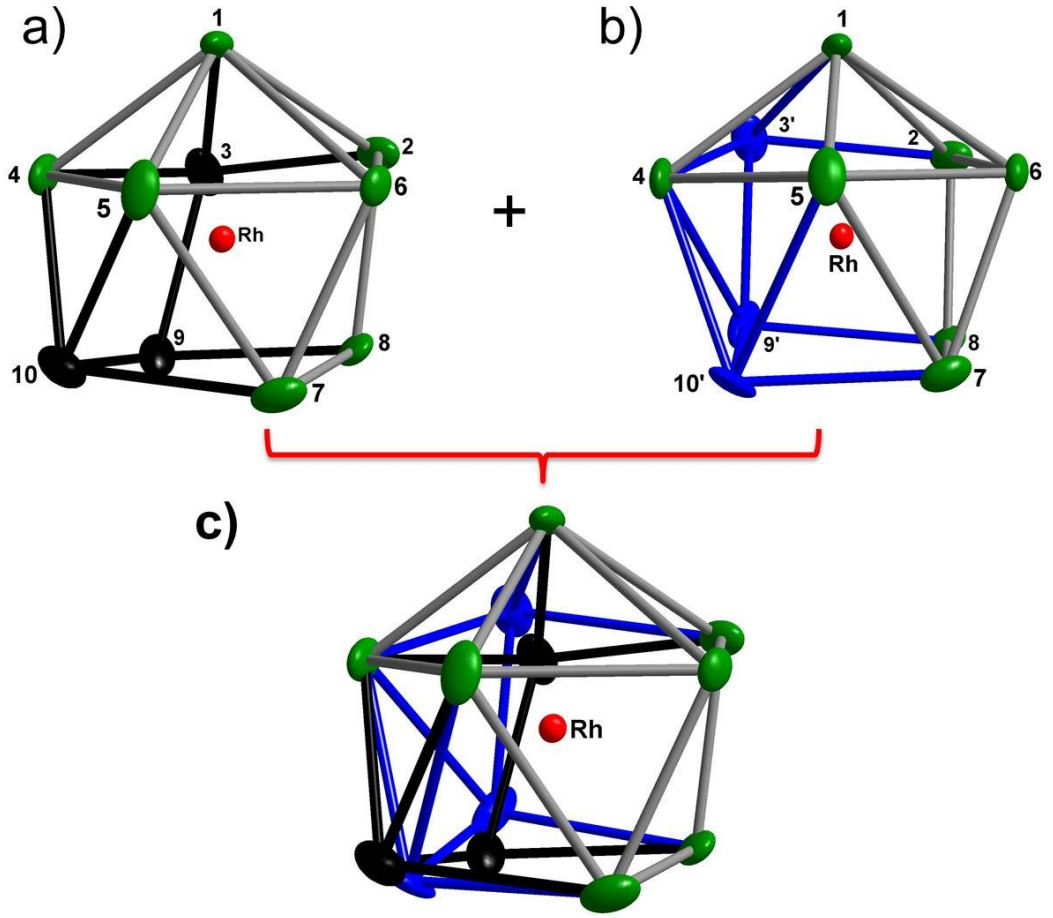

Figure S2. (a) Component 1 (62%) of the $[Rh@Sn_{10}]^{3-}$ anion. (b) Component 2 (38%). Displacement ellipsoids at the 50% level. (c) Disorder model illustrated by superposition of both compositions.

Compound **1** crystallises in the triclinic space group P-1, and contains one independent cluster sites in the asymmetric unit. Positional disorder was found in cluster site and was modeled accordingly. The cluster $[Rh@Sn_{10}]^{3-}$ adopts two different orientations, including a major component and a minor component. The occupancy of those two compositions were freely refined with the total site occupancy set to 100%, thus finally gave rise to a model with a 62:38 ratio of major to minor cluster site occupancy. The positions of 7 of the 10 Sn atoms are common to both major and minor components: only the positions of Sn(3/3'), Sn(9/9') and Sn(10/10') differ.

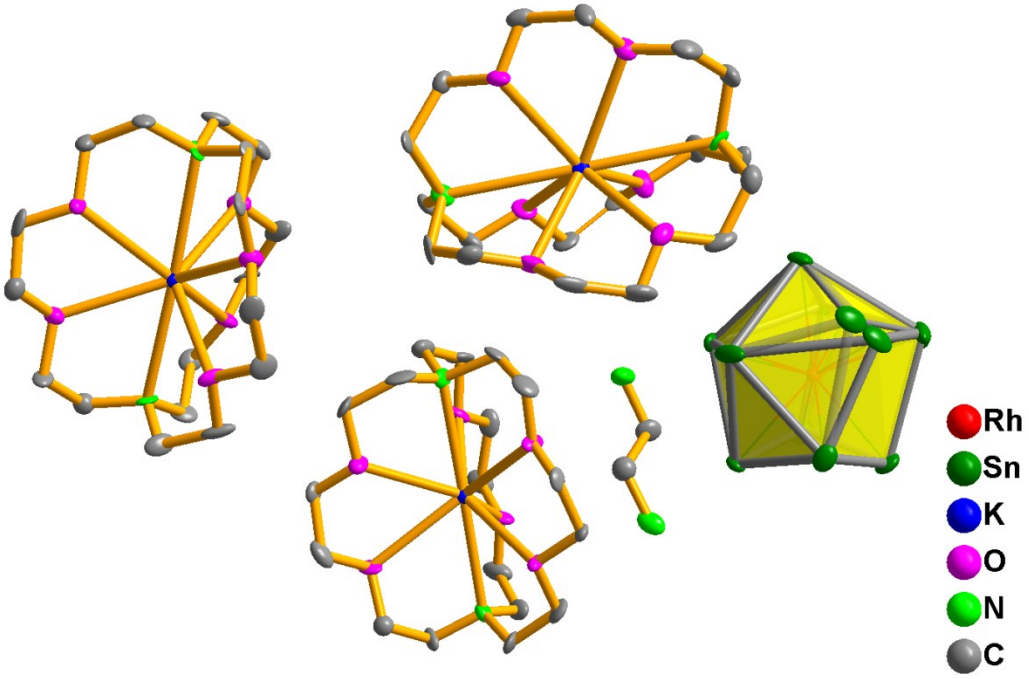

Figure S3. Asymmetric unit of **1.** Thermal ellipsoids are drawn at 50% probability. Solvent molecules and hydrogen atoms have been omitted for clarity.

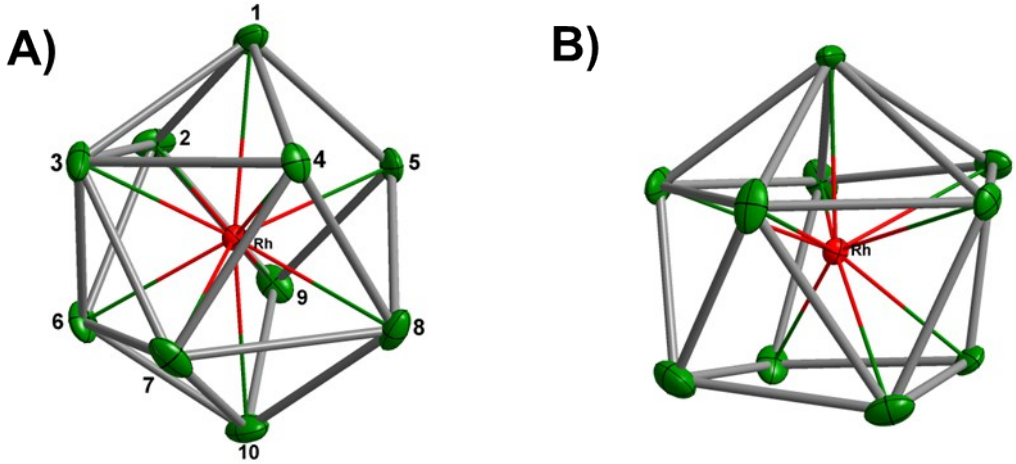

Figure S4. Two views of main component of the $[Rh@Sn_{10}]^{3-}$ (62%).

2.2 Structure of $[K(2,2,2\text{-crypt})]_3[Rh@Sn_{12}]$•Tol (2a)

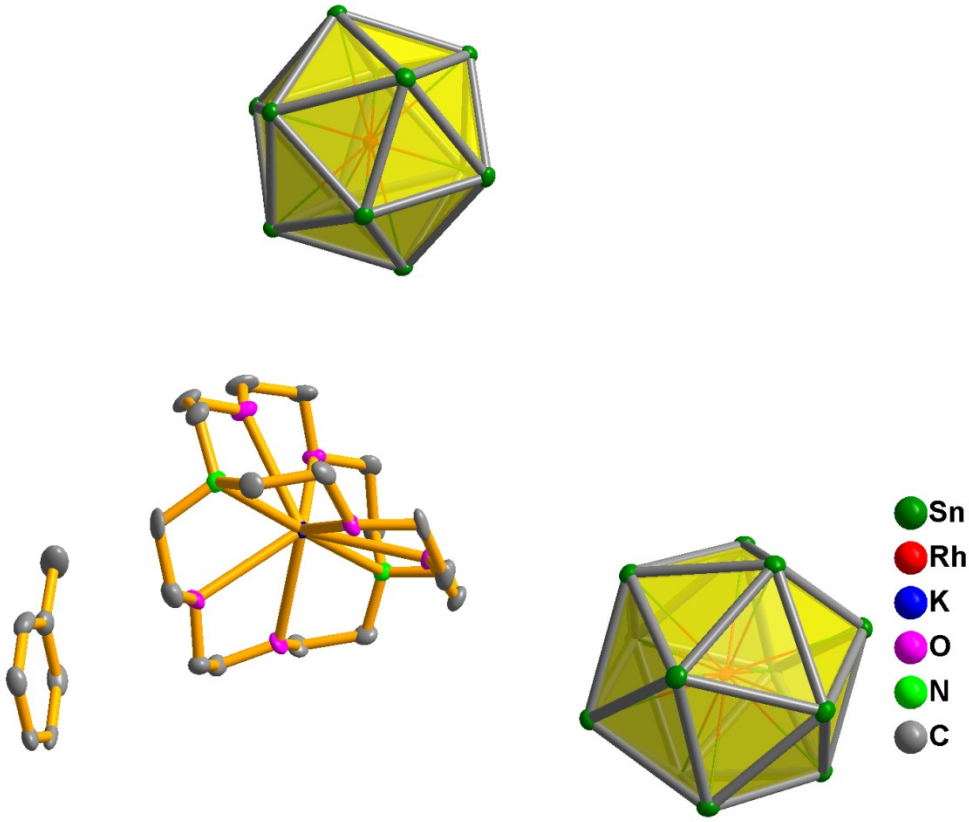

Figure S5. Asymmetric unit of **2a** with the cluster fragment expanded. Thermal ellipsoids are drawn at 50% probability. Solvent molecules and hydrogen atoms have been omitted for clarity.

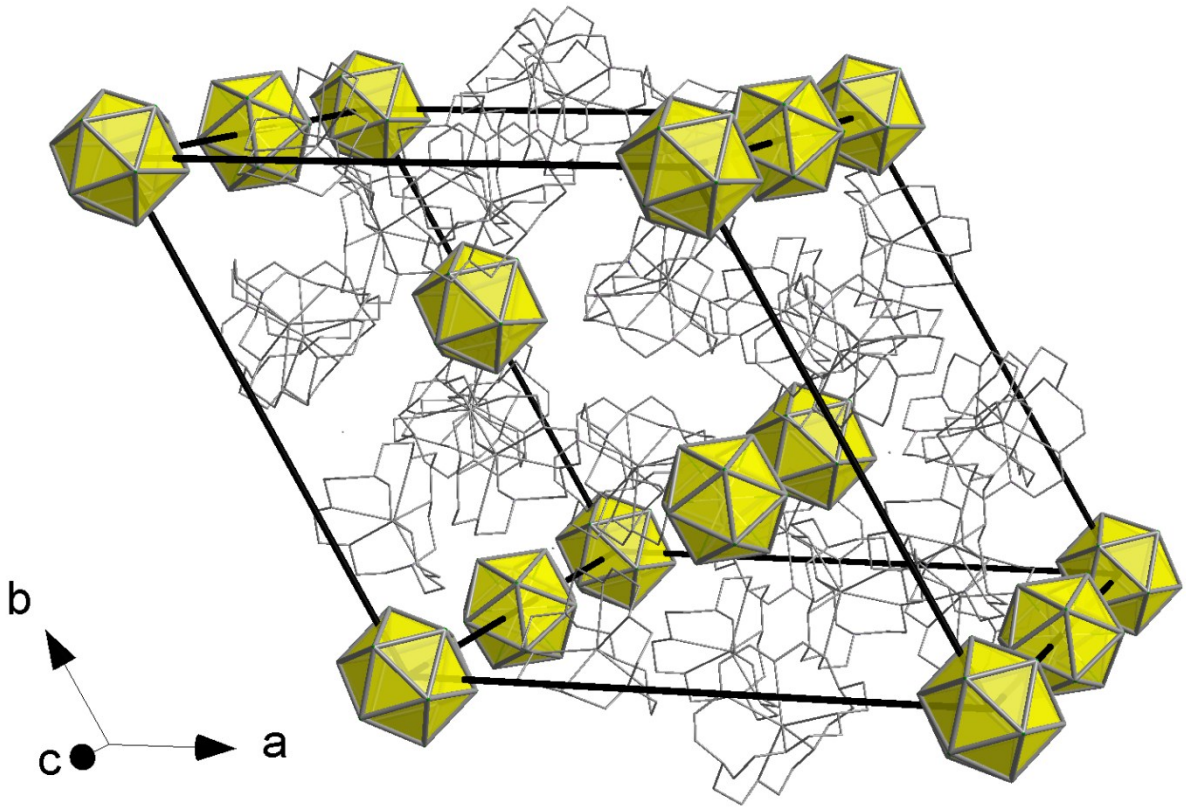

Figure S6. Packing of cations and anions in **2a.** Solvent molecules and hydrogen atoms are omitted for clarity.

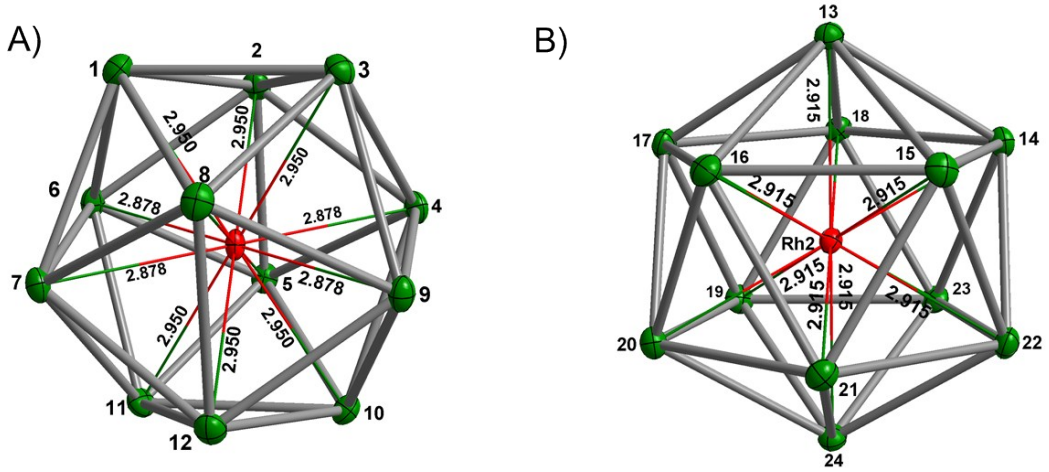

Figure S7. Thermal ellipsoid plots of the D_{3d}- (**A**) and I_h- (**B**) $[Rh@Sn_{12}]^{3-}$ anion in **2a**.

2.3 Structure of $\{K_3[K(2,2,2\text{-crypt})]_3[Rh_2@Sn_{17}]\}\bullet 4en$ (3)

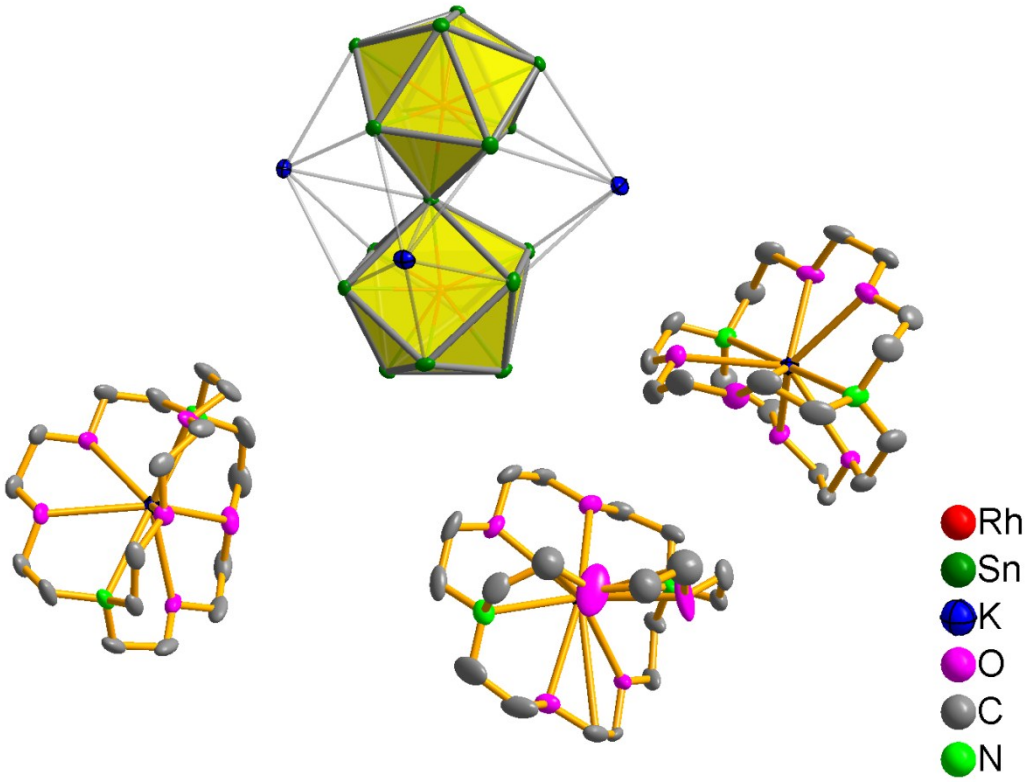

Figure S8. Asymmetric unit of **3**. Thermal ellipsoids are drawn at 50% probability. Solvent molecules and hydrogen atoms have been omitted for clarity.

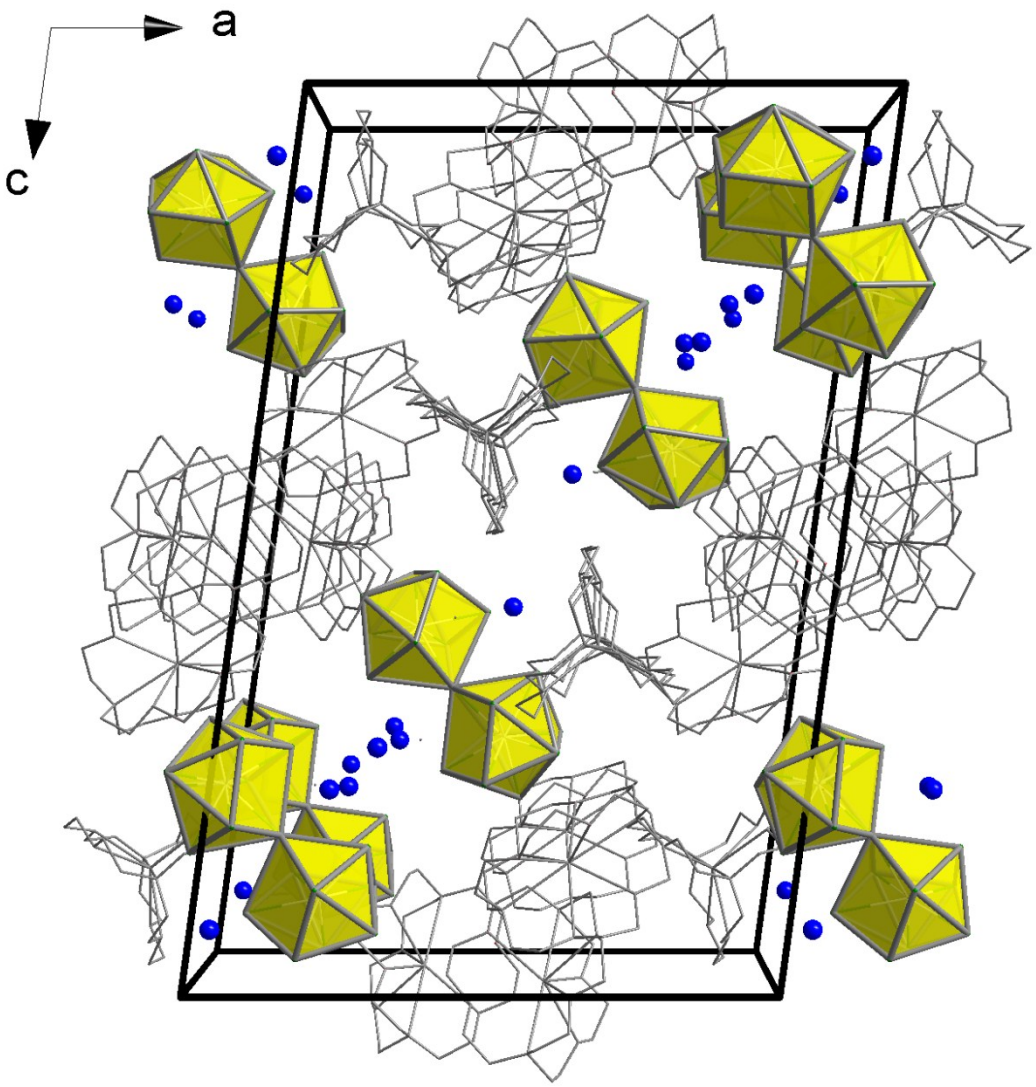

Figure S9 Packing of cations and anions in **3** viewed down the *b* axes. Solvent molecules and hydrogen atoms are omitted for clarity.

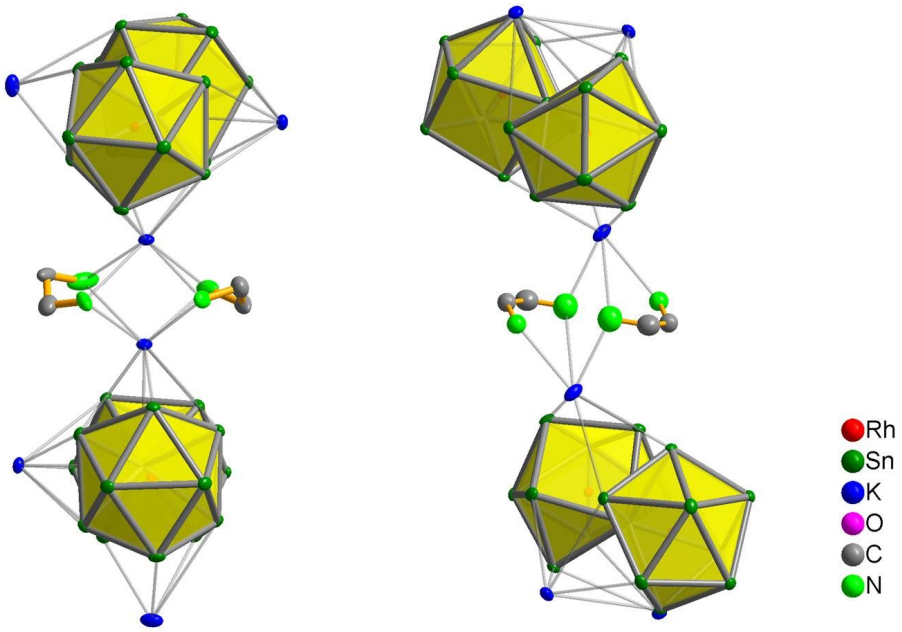

Figure S10. The coordination mode of the en molecules in the compound **3.**

2.4 Structure of $[K(2,2,2\text{-crypt})]_5[Rh_3@Sn_{24}]$•2DMF•Tol. (4)

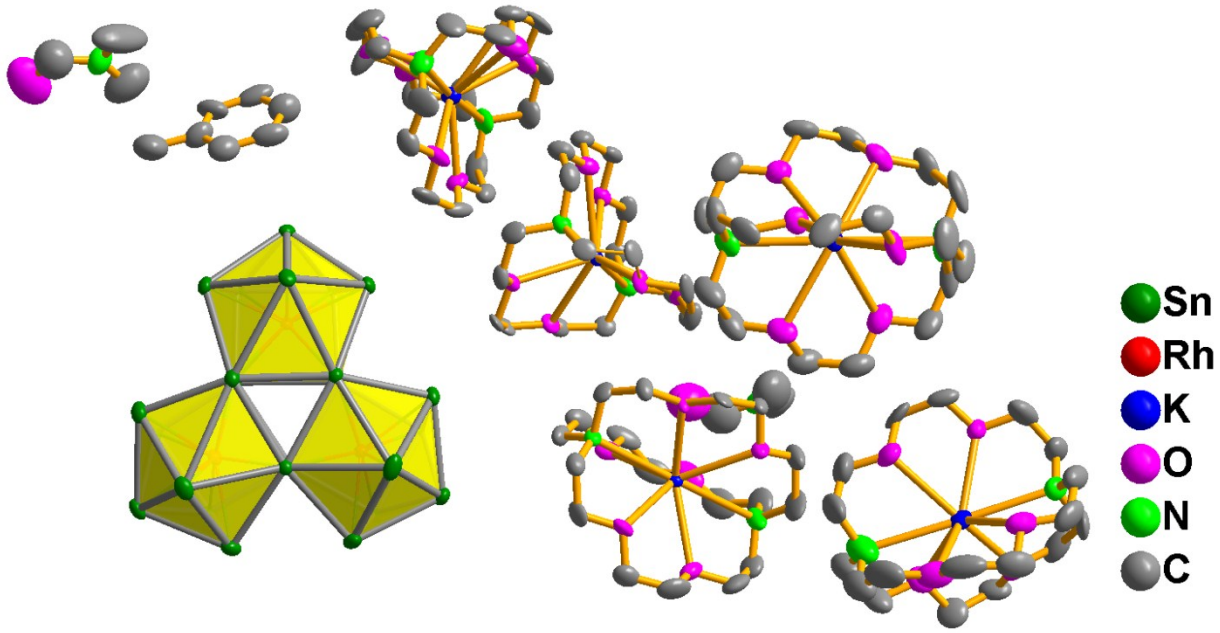

Figure S11. Asymmetric unit of **4**. Thermal ellipsoids are drawn at 50% probability. Solvent molecules and hydrogen atoms have been omitted for clarity.

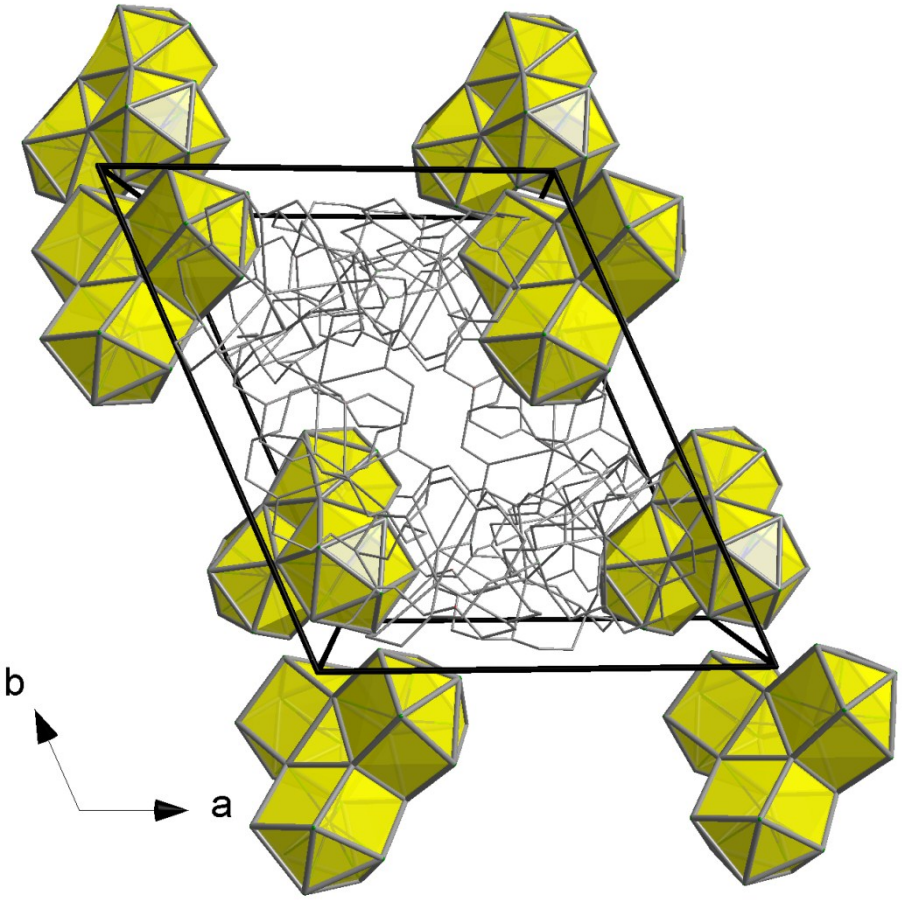

Figure S12. Packing of cations and anions in**4** viewed down the *a* axes. Solvent molecules and hydrogen atoms are omitted for clarity.

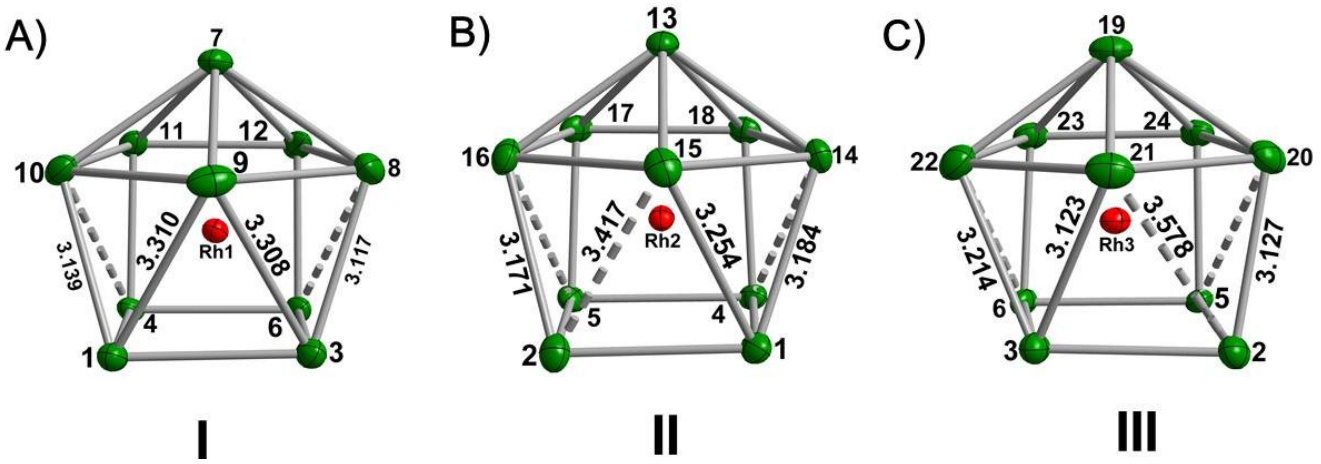

Figure S13. A)-C) ORTEP drawing of three Rh@Sn_{10}-subunits in $[Rh_3@Sn_{24}]^{5-}$, labeled as Ⅰ, Ⅱ and Ⅲ respectively.

2.5 Structure of $[K(2,2,2\text{-crypt})]_3[Rh@Sn_{12}]$•2DMF. (2b)

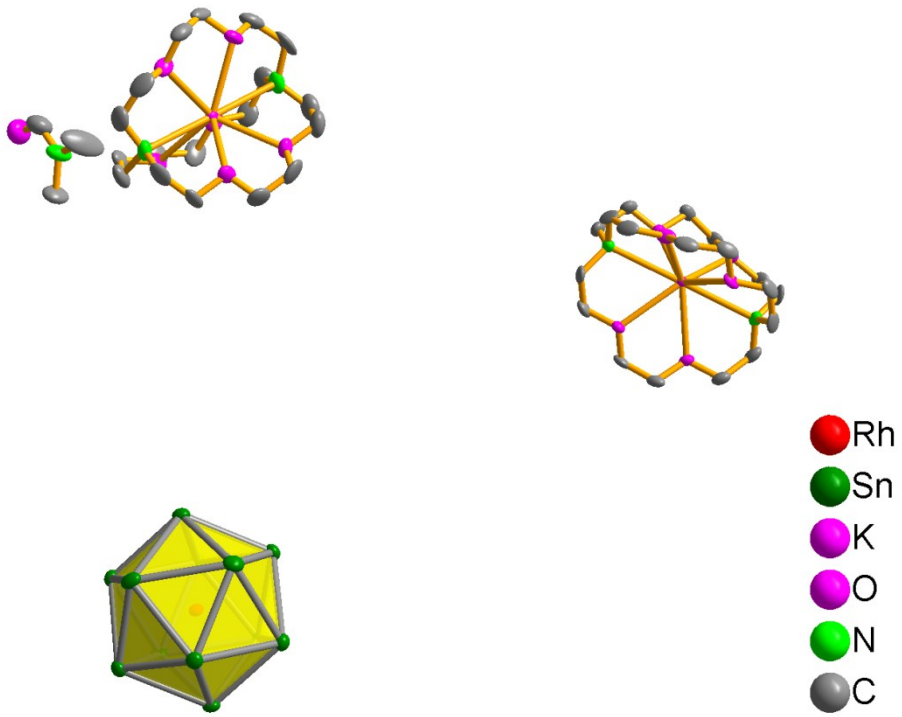

Figure S14. Asymmetric unit of **2b**. Thermal ellipsoids are drawn at 50% probability.

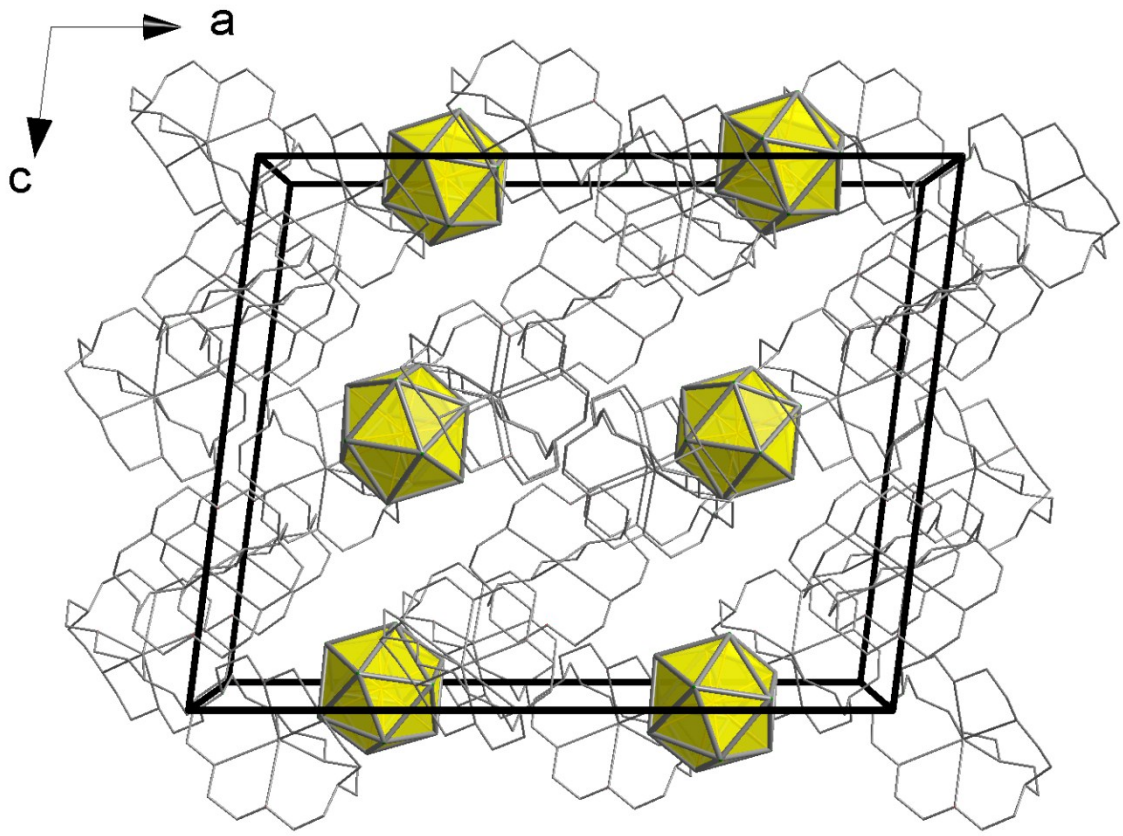

Figure S15. Packing of cations and anions in **2b** viewed down the *b* axes. Solvent molecules and hydrogen atoms are omitted for clarity.

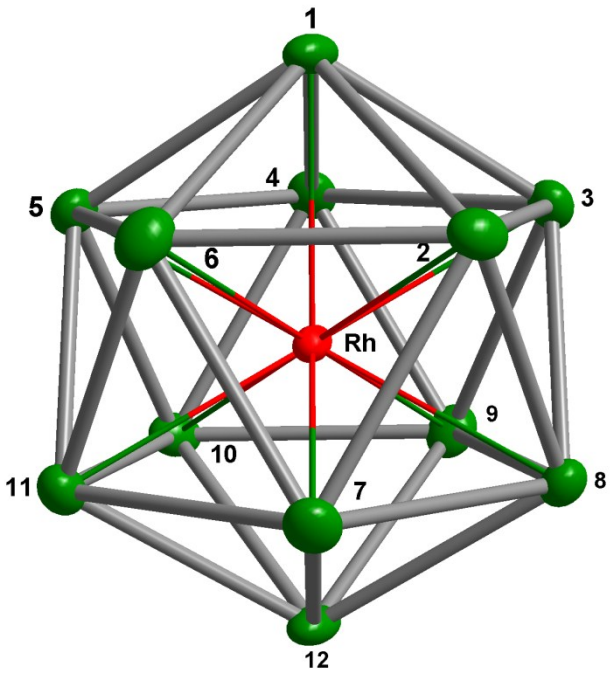

Figure S16. Thermal ellipsoid plots of the $[Rh@Sn_{12}]^{3-}$ anion in compound 2b. Like the D_{3d} -symmetric anion in 2a, this cluster is also distorted away from the ideal I_h -symmetric geometry, with Rh-Sn bond lengths ranging from 2.898-2.952 Å (see Table S6).

In Tables S2 – S6：measured and computed bond lengths for clusters 1-4.

Table S2. Selected interatomic distances (in Å) of the experimental and optimized structures of **1**.

Major Composition		Minor Composition		
	X-ray		X-ray	Calculated

Sn(1)-Sn(2)	3.1843(16)	Sn(1)-Sn(2)	3.1843(16)	3.27
Sn(1)-Sn(3)	3.3420(5)	Sn(1)-Sn(3')	2.889(8)	3.27
Sn(1)-Sn(4)	3.1101(15)	Sn(1)-Sn(4)	3.1101(15)	3.21
Sn(1)-Sn(5)	3.0257(17)	Sn(1)-Sn(5)	3.0257(17)	3.09
Sn(1)-Sn(6)	3.1470(15)	Sn(1)-Sn(6)	3.1470(15)	3.21
Sn(2)-Sn(3)	2.9957(5)	Sn(2)-Sn(3')	3.177(7)	3.12
Sn(2)-Sn(6)	2.909(3)	Sn(2)-Sn(6)	2.909(3)	3.06
Sn(2)-Sn(8)	2.9057(16)	Sn(2)-Sn(8)	2.9057(16)	2.96
Sn(3)-Sn(4)	3.122(5)	Sn(3')-Sn(4)	2.817(5)	3.06
Sn(3)-Sn(9)	2.974(4)	Sn(3')-Sn(9)	2.918(7)	2.96
Sn(4)-Sn(5)	3.1517(15)	Sn(4)-Sn(5)	3.1517(15)	3.21
Sn(4)-Sn(10)	2.915(5)	Sn(4)-Sn(10')	3.080(7)	3.06
Sn(5)-Sn(6)	3.0772(15)	Sn(4)-Sn(9')	3.279(5)	3.21
Sn(5)-Sn(7)	3.2138(16)	Sn(5)-Sn(7)	3.2138(16)	3.27
Sn(5)-Sn(10)	3.027(6)	Sn(5)-Sn(10)	3.027(6)	3.27
Sn(6)-Sn(7)	2.9689(16)	Sn(6)-Sn(7)	2.9689(16)	3.06
Sn(7)-Sn(10)	3.044(5)	Sn(7)-Sn(10')	3.149(5)	3.12
Sn(8)-Sn(9)	3.064(4)	Sn(8)-Sn(9')	2.7185(5)	3.40
Sn(9)-Sn(10)	2.914(4)	Sn(9')-Sn(10')	2.958(8)	2.95
Rh(1)-Sn(1)	2.7080(15)	Rh(1)-Sn(1)	2.7080(15)	2.77
Rh(1)-Sn(2)	2.8685(14)	Rh(1)-Sn(2)	Rh(1)-Sn(2)	2.90
Rh(1)-Sn(3)	2.709(3)	Rh(1)-Sn(3')	3.341(10)	2.90
Rh(1)-Sn(4)	2.7075(15)	Rh(1)-Sn(4)	2.7075(15)	2.82
Rh(1)-Sn(5)	2.7032(14)	Rh(1)-Sn(5)	2.7032(14)	2.77
Rh(1)-Sn(6)	2.7296(14)	Rh(1)-Sn(6)	2.7296(14)	2.82
Rh(1)-Sn(7)	2.7870(14)	Rh(1)-Sn(7)	2.7870(14)	2.90
Rh(1)-Sn(8)	2.6792(14)	Rh(1)-Sn(8)	2.6792(14)	2.75
Rh(1)-Sn(9)	2.706(3)	Rh(1)-Sn(9')	2.670(5)	2.75
Rh(1)-Sn(10)	2.887(4)	Rh(1)-Sn(10')	2.751(7)	2.90

Table S3. Selected interatomic distances (in angstroms) of the experimental and optimized structures of $[Rh@Sn_{12}]^{3-}$ in **2a.**

I_h -symmetric cluster		D_{3d} -symmetric cluster		
	Experiment		Experiment	Calculated
Sn(1)-Sn(2)	3.041(5)	Sn(13)-Sn(14)	3.0500(8)	3.15
Sn(1)-Sn(3)	3.041(5)	Sn(13)-Sn(15)	3.0763(6)	
Sn(1)-Sn(6)	3.0622(7)	Sn(13)-Sn(16)	3.0748(7)	
Sn(1)-Sn(7)	3.1290(7)	Sn(13)-Sn(17)	3.0560(6)	
Sn(1)-Sn(8)	3.0438(5)	Sn(13)-Sn(18)	3.0500(8)	

Sn(2)-Sn(3)	3.041(5)	Sn(14)-Sn(15)	3.0646(5)	
Sn(2)-Sn(4)	3.0622(7)	Sn(14)-Sn(18)	3.0500(8)	
Sn(2)-Sn(5)	3.1290(7)	Sn(14)-Sn(22)	3.0748(7)	
Sn(2)-Sn(6)	3.0438(5)	Sn(14)-Sn(23)	3.0763(6)	
Sn(3)-Sn(4)	3.0438(5)	Sn(15)-Sn(16)	3.0646(5)	
Sn(3)-Sn(8)	3.0622(7)	Sn(15)-Sn(21)	3.0748(7)	
Sn(3)-Sn(9)	3.1290(7)	Sn(15)-Sn(22)	3.0646(5)	
Sn(4)-Sn(5)	3.0438(5)	Sn(16)-Sn(17)	3.0646(5)	
Sn(4)-Sn(9)	3.0438(5)	Sn(16)-Sn(20)	3.0763(6)	
Sn(4)-Sn(10)	3.1290(7)	Sn(16)-Sn(21)	3.0560(7)	
Sn(5)-Sn(6)	3.0438(5)	Sn(17)-Sn(18)	3.0763(6)	
Sn(5)-Sn(10)	3.0437(7)	Sn(17)-Sn(20)	3.0748(7)	
Sn(5)-Sn(11)	3.0622(7)	Sn(17)-Sn(19)	3.0646(5)	
Sn(6)-Sn(7)	3.0438(5)	Sn(18)-Sn(19)	3.0748(7)	
Sn(6)-Sn(11)	3.1290(7)	Sn(18)-Sn(23)	3.0560(6)	
Sn(7)-Sn(8)	3.0438(5)	Sn(19)-Sn(20)	3.0560(6)	
Sn(7)-Sn(11)	3.0438(5)	Sn(19)-Sn(23)	3.0646(5)	
Sn(7)-Sn(12)	3.0622(7)	Sn(19)-Sn(24)	3.0763(6)	
Sn(8)-Sn(9)	3.0438(5)	Sn(20)-Sn(21)	3.0500(8)	
Sn(8)-Sn(12)	3.1290(7)	Sn(20)-Sn(24)	3.0500(8)	
Sn(9)-Sn(10)	3.0622(7)	Sn(21)-Sn(22)	3.0763(6)	
Sn(9)-Sn(12)	3.0437(7)	Sn(21)-Sn(24)	3.0500(8)	
Sn(10)-Sn(11)	3.041(5)	Sn(22)-Sn(23)	3.0646(5)	
Sn(10)-Sn(12)	3.041(5)	Sn(22)-Sn(24)	3.0560(6)	
Sn(11)-Sn(12)	3.041(5)	Sn(23)-Sn(24)	3.0748(7)	
Rh(1)-Sn(1)	2.9498(5)	Rh(2)-Sn(13)	2.9149(5)	2.99
Rh(1)-Sn(2)	2.9498(5)	Rh(2)-Sn(14)	2.9139(5)	
Rh(1)-Sn(3)	2.9498(5)	Rh(2)-Sn(15)	2.9149(5)	
Rh(1)-Sn(4)	2.8781(4)	Rh(2)-Sn(16)	2.9149(5)	
Rh(1)-Sn(5)	2.8780(5)	Rh(2)-Sn(17)	2.9148(5)	
Rh(1)-Sn(6)	2.8779(4)	Rh(2)-Sn(18)	2.9148(5)	
Rh(1)-Sn(7)	2.8781(4)	Rh(2)-Sn(19)	2.9149(5)	
Rh(1)-Sn(8)	2.8781(4)	Rh(2)-Sn(20)	2.9139(5)	
Rh(1)-Sn(9)	2.8781(4)	Rh(2)-Sn(21)	2.9139(4)	
Rh(1)-Sn(10)	2.9498(5)	Rh(2)-Sn(22)	2.9139(5)	
Rh(1)-Sn(11)	2.9498(5)	Rh(2)-Sn(23)	2.9139(5)	
Rh(1)-Sn(12)	2.9498(5)	Rh(1)-Sn(24)	2.9139(5)	

Table S4. Selected interatomic distances (in Å) of the experimental and optimized structures of **3.** Atom numbering is given in Figure 5 in the main text.

	X-ray	Calculated		X-ray	Calculated
Sn(1)-Sn(2)	3.1277(5)	3.21	Rh(1)-Sn(1)	2.7374(5)	2.76
Sn(1)-Sn(3)	3.0350(5)	3.13	Rh(1)-Sn(2)	2.7306(5)	2.76
Sn(1)-Sn(4)	3.1276(5)	3.34	Rh(1)-Sn(3)	2.7595(5)	2.79
Sn(1)-Sn(5)	3.3050(5)	3.34	Rh(1)-Sn(4)	2.7066(5)	2.78
Sn(1)-Sn(6)	3.0491(5)	3.13	Rh(1)-Sn(5)	2.7140(5)	2.78
Sn(2)-Sn(3)	2.9957(5)	3.13	Rh(1)-Sn(6)	2.7305(5)	2.79
Sn(2)-Sn(6)	3.0123(6)	3.13	Rh(1)-Sn(7)	2.7212(5)	2.78
Sn(2)-Sn(8)	3.2304(6)	3.34	Rh(1)-Sn(8)	2.7205(5)	2.78
Sn(3)-Sn(4)	3.0397(5)	3.10	Rh(1)-Sn(9)	2.4974(5)	2.52
Sn(3)-Sn(8)	3.1083(6)	3.10	Rh(2)-Sn(9)	2.4975(5)	2.52
Sn(4)-Sn(5)	3.0015(5)	3.05	Rh(2)-Sn(10)	2.7007(5)	2.78
Sn(4)-Sn(9)	3.2468(6)	3.28	Rh(2)-Sn(11)	2.7122(5)	2.78
Sn(5)-Sn(6)	3.0220(5)	3.10	Rh(2)-Sn(12)	2.6962(5)	2.78
Sn(5)-Sn(9)	3.2483(5)	2.28	Rh(2)-Sn(13)	2.7046(5)	2.78
Sn(6)-Sn(7)	3.0327(6)	3.10	Rh(2)-Sn(14)	2.7607(5)	2.79
Sn(7)-Sn(8)	2.9333(5)	3.05	Rh(2)-Sn(15)	2.7456(5)	2.76
Sn(8)-Sn(9)	3.2754(6)	3.28	Rh(2)-Sn(16)	2.7541(5)	2.76
Sn(9)-Sn(10)	3.2216(5)	3.28	Rh(2)-Sn(17)	2.7185(5)	2.79
Sn(9)-Sn(11)	3.2382(5)	3.28	K(1)-Sn(4)	3.682	
Sn(9)-Sn(12)	3.2397(5)	3.28	K(1)-Sn(5)	3.779	
Sn(10)-Sn(11)	2.9994(5)	3.05	K(1)-Sn(11)	3.817	
Sn(10)-Sn(14)	3.0092(5)	3.10	K(1)-Sn(12)	3.770	
Sn(11)-Sn(15)	3.1118(5)	3.10	K(1)-Sn(16)	3.684	
Sn(11)-Sn(16)	3.0312(5)	3.10	K(2)-Sn(3)	3.781	
Sn(12)-Sn(13)	2.9773(5)	3.05	K(2)-Sn(4)	3.834	
Sn(12)-Sn(16)	3.1202(6)	3.10	K(2)-Sn(10)	3.728	
Sn(12)-Sn(17)	3.2091(5)	3.34	K(2)-Sn(11)	3.598	
Sn(13)-Sn(14)	3.0069(5)	3.10	K(2)-Sn(8)	3.787	
Sn(14)-Sn(15)	3.0513(5)	3.13	K(3)-Sn(5)	4.011	
Sn(14)-Sn(17)	3.0418(6)	3.13	K(3)-Sn(6)	3.780	
Sn(15)-Sn(16)	3.0130(5)	3.13	K(3)-Sn(7)	3.973	
Sn(15)-Sn(17)	3.1613(5)	3.21	K(3)-Sn(12)	3.756	
Sn(16)-Sn(17)	3.0050(6)	3.13	K(3)-Sn(13)	3.659	

Table S5. Selected interatomic distances (in Å) of the experimental and optimized structures of **4**$^{-}$.

	Experiment	Calculated		Experiment	Calculated
Sn(1)-Sn(2)	3.0536(10)	3.15	Sn(7)-Rh(1)	2.7961(11)	2.89
Sn(1)-Sn(3)	3.0910(10)	3.15	Sn(8)-Sn(9)	3.1231(14)	3.12

Sn(1)-Sn(4)	3.1896(10)	3.21	Sn(8)-Sn(12)	2.9730(13)	3.07
Sn(1)-Sn(9)	3.3102(10)	3.41	Sn(8)-Rh(1)	2.7853(11)	2.83
Sn(1)-Sn(10)	3.1392(10)	3.24	Sn(9)-Sn(10)	3.0554(12)	3.12
Sn(1)-Sn(14)	3.1836(10)	3.24	Sn(9)-Rh(1)	2.7273(11)	2.78
Sn(1)-Sn(15)	3.2540(11)	3.41	Sn(10)-Sn(11)	2.9666(10)	3.07
Sn(1)-Rh(1)	2.9189(10)	2.93	Sn(10)-Rh(1)	2.7817(11)	2.83
Sn(1)-Rh(2)	2.8378(10)	2.93	Sn(11)-Sn(12)	2.9890(11)	3.05
Sn(2)-Sn(3)	3.0669(10)	3.15	Sn(11)-Rh(1)	2.9125(10)	2.99
Sn(2)-Sn(5)	3.1275(10)	3.21	Sn(12)-Rh(1)	2.9044(11)	2.99
Sn(2)-Sn(15)	3.4170(10)	3.41	Sn(13)-Sn(14)	3.0621(10)	3.12
Sn(2)-Sn(16)	3.1706(11)	3.24	Sn(13)-Sn(15)	3.0223(11)	3.10
Sn(2)-Sn(20)	3.1274(11)	3.24	Sn(13)-Sn(16)	3.0829(11)	3.12
Sn(2)-Sn(21)	3.5780(10)	3.41	Sn(13)-Sn(17)	3.0367(10)	3.10
Sn(2)-Rh(2)	2.9836(11)	2.93	Sn(13)-Sn(18)	3.0401(10)	3.10
Sn(2)-Rh(3)	3.0587(11)	2.93	Sn(13)-Rh(2)	2.8077(10)	2.89
Sn(3)-Sn(6)	3.1789(10)	3.21	Sn(14)-Sn(15)	3.0433(10)	3.12
Sn(3)-Sn(8)	3.1173(11)	3.24	Sn(14)-Sn(18)	3.0063(10)	3.07
Sn(3)-Sn(9)	3.3080(10)	3.41	Sn(14)-Rh(2)	2.7628(10)	2.83
Sn(3)-Sn(21)	3.1235(11)	3.41	Sn(15)-Sn(16)	3.0322(11)	3.12
Sn(3)-Sn(22)	3.2137(11)	3.24	Sn(15)-Rh(2)	2.7103(10)	2.78
Sn(3)-Rh(1)	2.7875(10)	2.93	Sn(16)-Sn(17)	2.9961(11)	3.07
Sn(3)-Rh(3)	2.7530(11)	2.93	Sn(16)-Rh(2)	2.7484(10)	2.83
Sn(4)-Sn(5)	3.1811(10)	3.16	Sn(17)-Sn(18)	2.9879(11)	3.05
Sn(4)-Sn(6)	3.0259(10)	3.16	Sn(18)-Rh(2)	2.9205(10)	2.99
Sn(4)-Sn(11)	3.0133(10)	3.07	Sn(19)-Sn(20)	3.0735(12)	3.12
Sn(4)-Sn(18)	2.9638(10)	3.07	Sn(19)-Sn(21)	3.0252(12)	3.10
Sn(4)-Rh(1)	2.6810(10)	2.75	Sn(19)-Sn(22)	3.0751(12)	3.12
Sn(4)-Rh(2)	2.6992(10)	2.75	Sn(19)-Sn(23)	3.0350(11)	3.10
Sn(5)-Sn(6)	3.1096(10)	3.16	Sn(19)-Sn(24)	3.0472(11)	3.10
Sn(5)-Sn(17)	3.0076(10)	3.07	Sn(19)-Rh(3)	2.7909(11)	2.89
Sn(5)-Sn(24)	3.0008(10)	3.07	Sn(20)-Sn(21)	3.0635(12)	3.12
Sn(5)-Rh(2)	2.6585(10)	2.75	Sn(20)-Sn(24)	3.0120(11)	3.07
Sn(5)-Rh(3)	2.6569(10)	2.75	Sn(20)-Rh(3)	2.7484(11)	2.83
Sn(6)-Sn(12)	2.9948(11)	3.07	Sn(21)-Sn(22)	3.0425(12)	3.12
Sn(6)-Sn(23)	2.9763(11)	3.07	Sn(21)-Rh(3)	2.7352(11)	2.78
Sn(6)-Rh(1)	2.7254(11)	2.75	Sn(22)-Sn(23)	2.9896(11)	3.07
Sn(6)-Rh(3)	2.7018(11)	2.75	Sn(22)-Rh(3)	2.7845(11)	2.83
Sn(7)-Sn(8)	3.0640(12)	3.12	Sn(23)-Sn(24)	2.9894(11)	3.05
Sn(7)-Sn(9)	3.0029(12)	3.10	Sn(23)-Rh(3)	2.9009(11)	2.99

Sn(7)-Sn(10)	3.0825(11)	3.12	Sn(24)-Rh(3)	2.8914(11)	2.99
Sn(7)-Sn(11)	3.0363(11)	3.12			
Sn(7)-Sn(12)	3.0445(12)	3.12			

Table S6. Selected interatomic distances (in Å) of the X-ray and optimized structures of the $[Rh@Sn_{12}]^{3-}$ anion in compound **2b**.

	X-ray	Calculated		Experiment	Calculated
Sn(1)-Sn(2)	3.0631(9)	3.15	Rh(1)-Sn(1)	2.9518(6)	2.99
Sn(1)-Sn(3)	3.0618(8)		Rh(1)-Sn(12)	2.9517(6)	
Sn(1)-Sn(4)	3.0754(9)		Rh(1)-Sn(8)	2.9206(6)	
Sn(1)-Sn(5)	3.0557(8)		Rh(1)-Sn(2)	2.9205(6)	
Sn(1)-Sn(6)	3.0960(9)		Rh(1)-Sn(7)	2.9057(6)	
Sn(2)-Sn(3)	3.0674(9)		Rh(1)-Sn(3)	2.9056(6)	
Sn(2)-Sn(10)	3.1034(10)		Rh(1)-Sn(11)	2.9241(7)	
Sn(2)-Sn(11)	3.1017(8)		Rh(1)-Sn(4)	2.9240(7)	
Sn(2)-Sn(6)	3.0411(9)		Rh(1)-Sn(10)	2.8984(7)	
Sn(3)-Sn(4)	3.0400(9)		Rh(1)-Sn(5)	2.8984(7)	
Sn(3)-Sn(9)	3.0858(9)		Rh(1)-Sn(9)	2.9296(7)	
Sn(3)-Sn(10)	3.0842(9)		Rh(1)-Sn(6)	2.9295(7)	
Sn(4)-Sn(8)	3.1017(8)				
Sn(4)-Sn(5)	3.0618(8)				
Sn(4)-Sn(9)	3.0696(8)				
Sn(5)-Sn(7)	3.0842(9)				
Sn(5)-Sn(8)	3.1034(10)				
Sn(5)-Sn(6)	3.0733(8)				
Sn(6)-Sn(11)	3.0696(8)				
Sn(6)-Sn(7)	3.0858(9)				
Sn(7)-Sn(8)	3.0674(9)				
Sn(7)-Sn(11)	3.0400(9)				
Sn(7)-Sn(12)	3.0618(8)				
Sn(8)-Sn(9)	3.0411(9)				
Sn(8)-Sn(12)	3.0631(9)				
Sn(9)-Sn(10)	3.0733(8)				
Sn(9)-Sn(12)	3.0960(9)				
Sn(10)-Sn(11)	3.0618(8)				
Sn(10)-Sn(12)	3.0557(8)				
Sn(11)-Sn(12)	3.0754(9)				

3. ESI-MS Studies

3.1 Detailed ESI mass spectrum of the en reaction mixtures.

The ESI mass spectrum of the en resulting mixture in Figure 17 shows a dominant peak corresponding to $[RhSn_{10}]^-$ (m/z = 1289.93) along with smaller peaks due to $[RhSn_{12}]^-$ (m/z = 1527.75), $[RhSn_8]^-$ (m/z = 1052.14), $[RhSn_9]^-$ (m/z = 1171.01), $\{(K(2,2,2\text{-crypt})[RhSn_{12}]\}^-$ (m/z = 1942.91), $[Rh_2Sn_{17}]^-$ (m/z = 2225.12) and $[K_3Rh_2Sn_{17}]^-$ (m/z = 2342.00). Measured and simulated isotope distributions for all four species are shown in the supporting information, Figures S18-24.

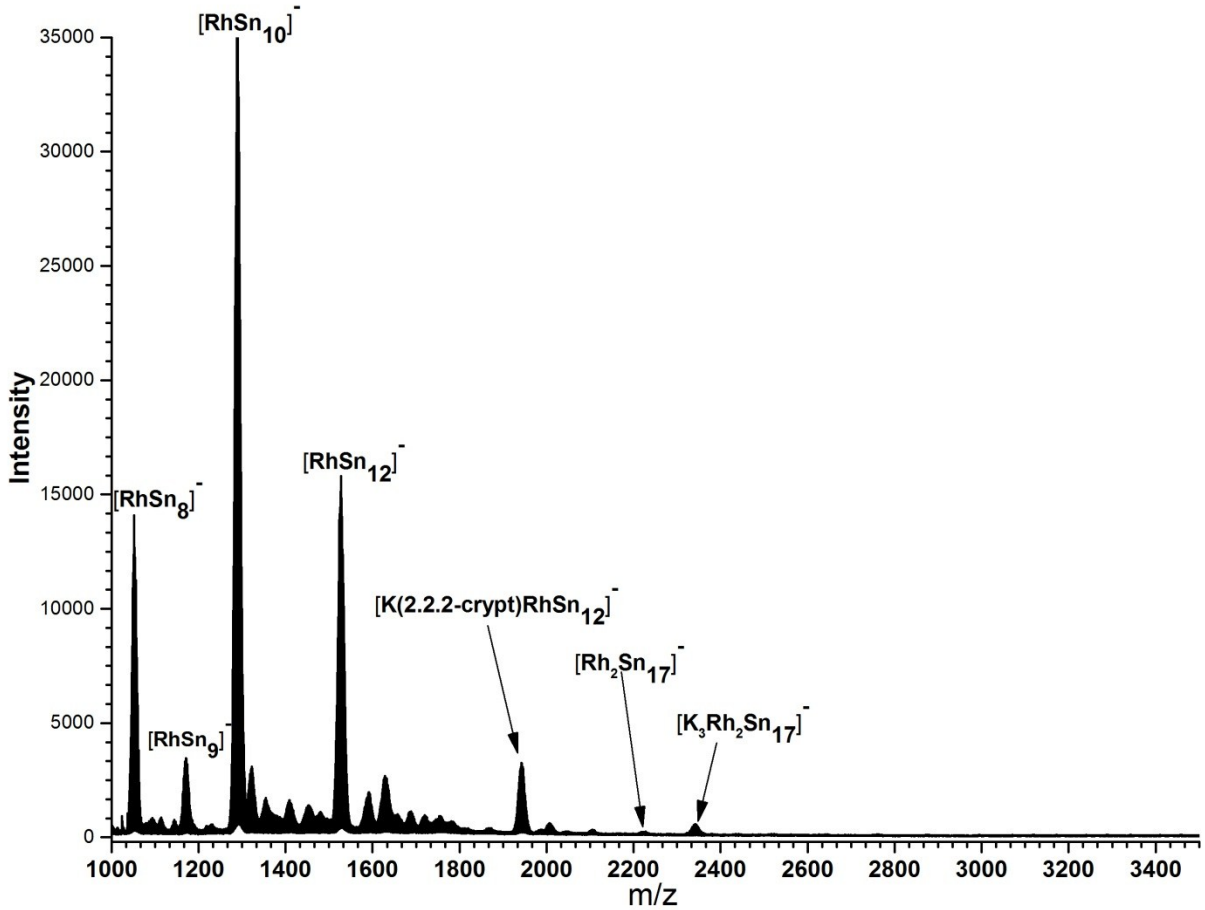

Figure S17. Overview ESI mass spectrum negative ion mode of the en reaction mixtures.

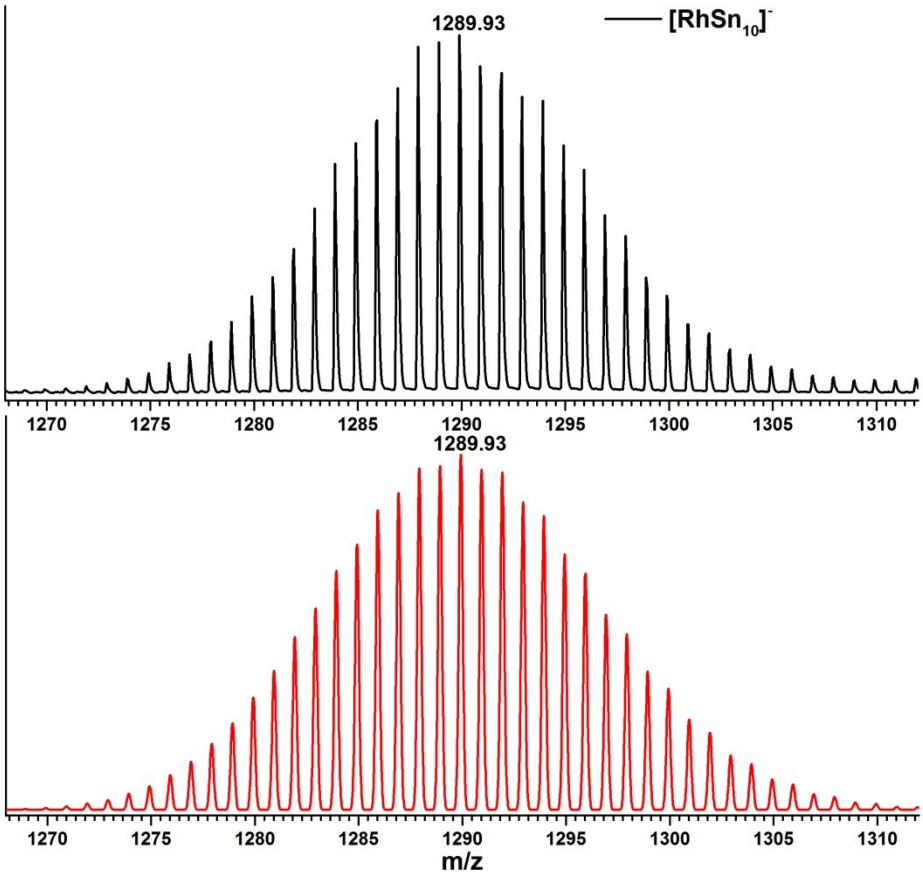

Figure S18. Measured (top) and simulated (bottom) spectrum of the fragment $[RhSn_{10}]^-$.

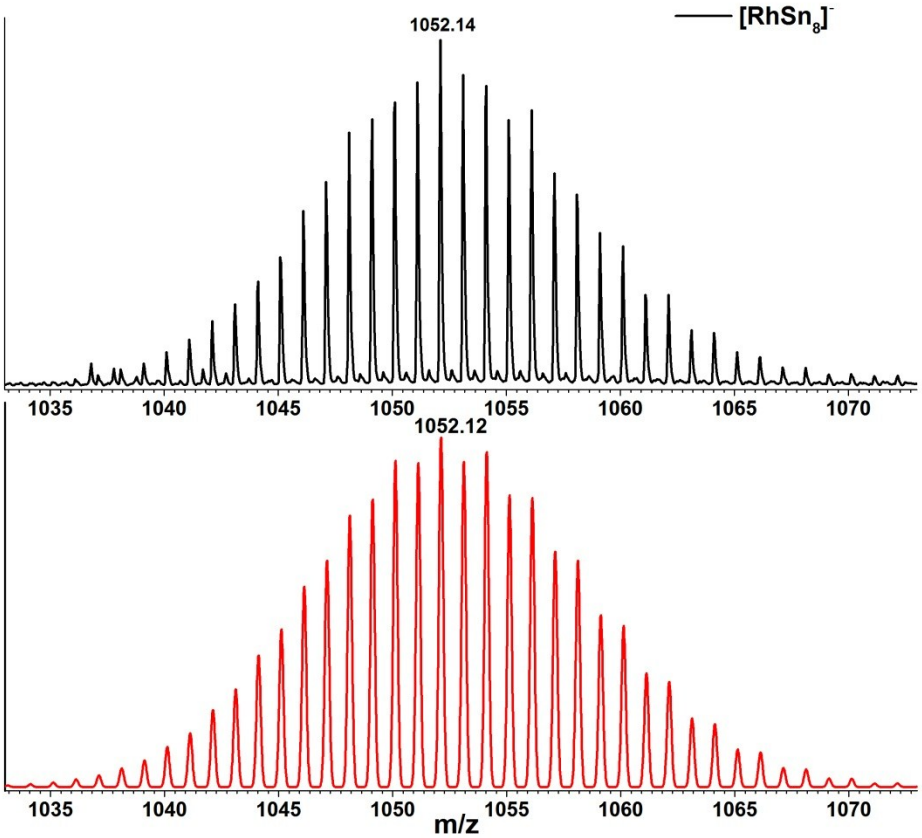

Figure S19. Measured (top) and simulated (bottom) spectrum of the fragment $[RhSn_8]^-$.

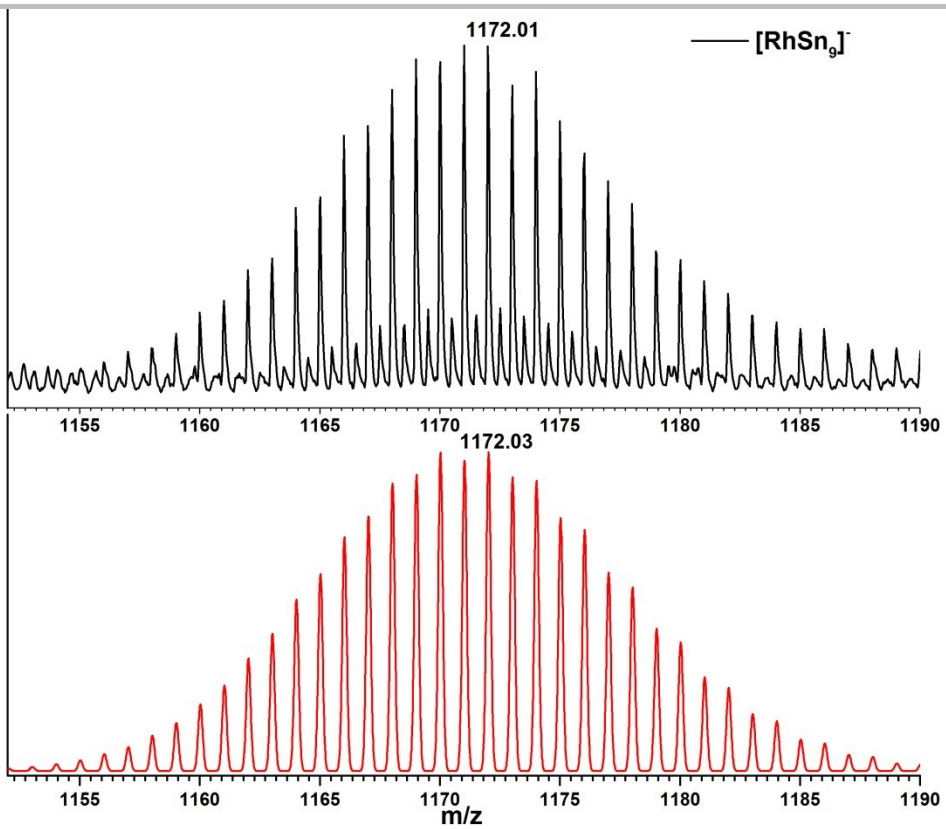

Figure S20. Measured (top) and simulated (bottom) spectrum of the fragment $[RhSn_9]^-$.

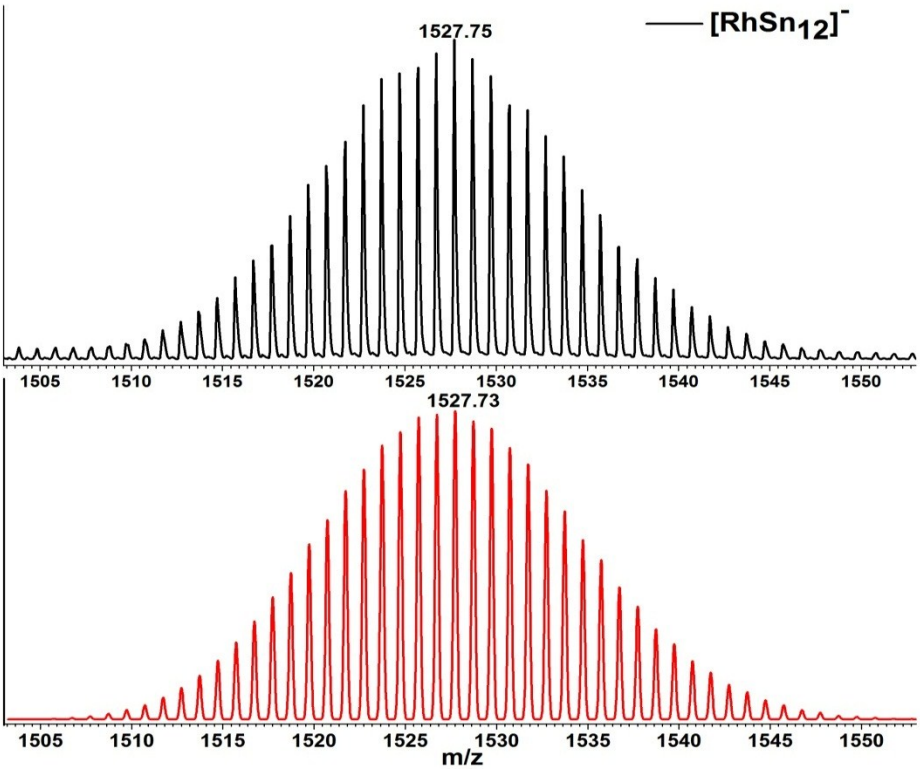

Figure S21. Measured (top) and simulated (bottom) spectrum of the fragment $[RhSn_{12}]^-$.

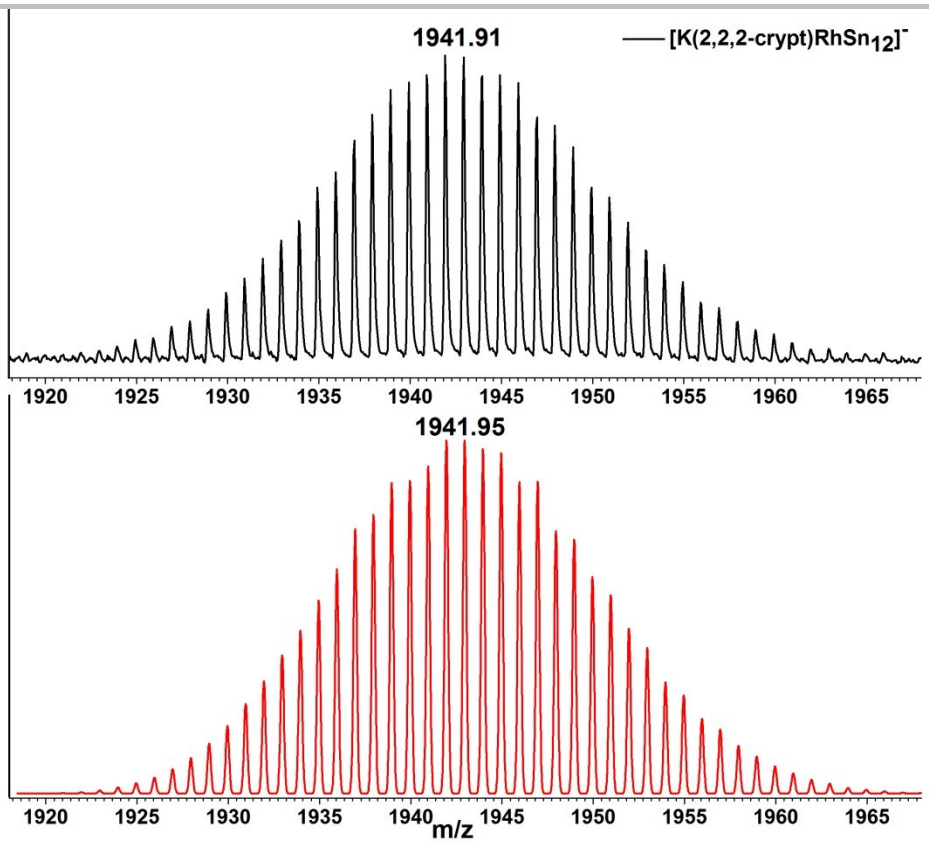

Figure S22. Measured (top) and simulated (bottom) spectrum of the fragment $[K(2,2,2\text{-crypt})RhSn_{12}]^-$.

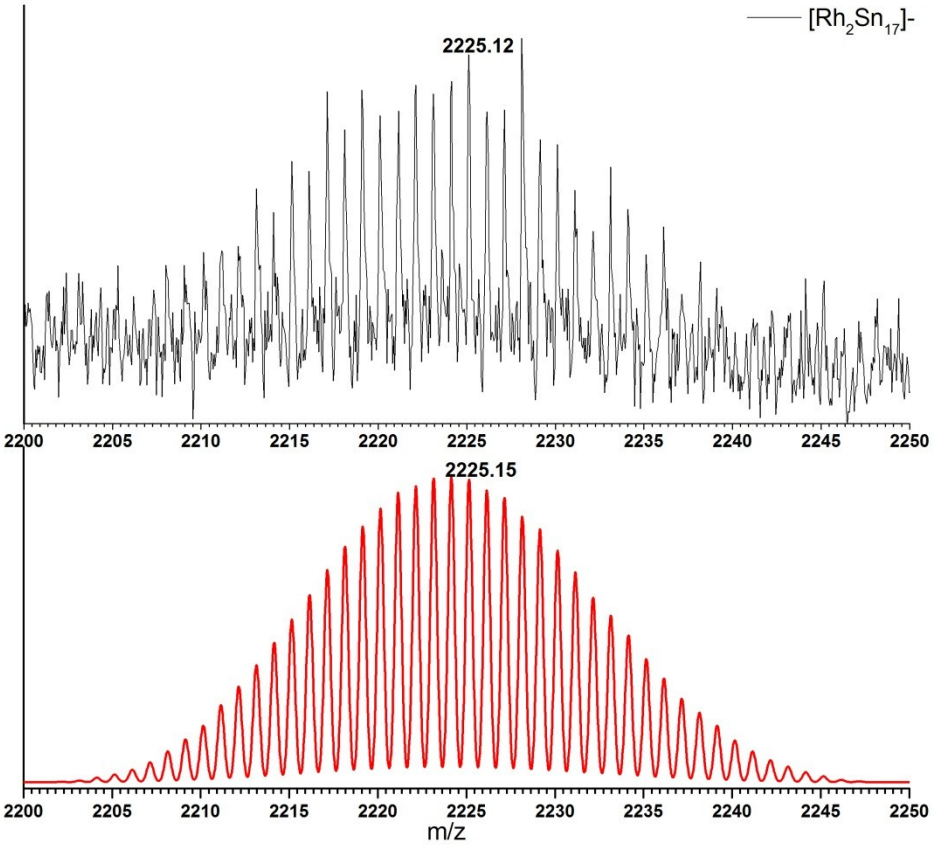

Figure S23. Measured (top) and simulated (bottom) spectrum of the fragment $[Rh_2Sn_{17}]^-$.

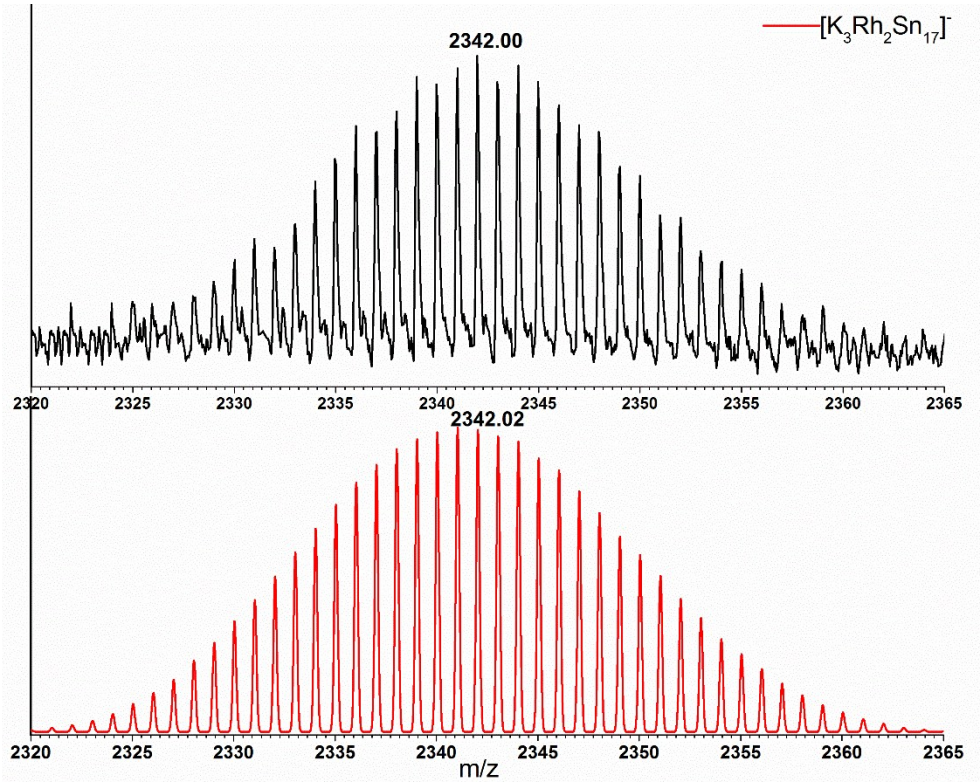

Figure S24. Measured (top) and simulated (bottom) spectrum of the fragment $[K_3Rh_2Sn_{17}]^-$.

3.2 Detailed ESI mass spectrum of the DMF reaction mixtures.

The ESI-MS experiments on the DMF reaction mixture indicate that the potassium adduct $\{K[Rh_3Sn_{24}]\}^-$(m/z= 3196) is stable in solution (Figure 25). The other dominant species in the ESI-MS is $[RhSn_{12}]^-$ (m/z = 1527.70), $\{(K(2,2,2\text{-crypt})[RhSn_{12}]\}^-$ (m/z = 1942.95) along with smaller amounts of $[RhSn_{10}]^-$ (m/z = 1290.00). Measured and simulated isotope distributions for all four species are shown in the supporting information, Figures S26-29.

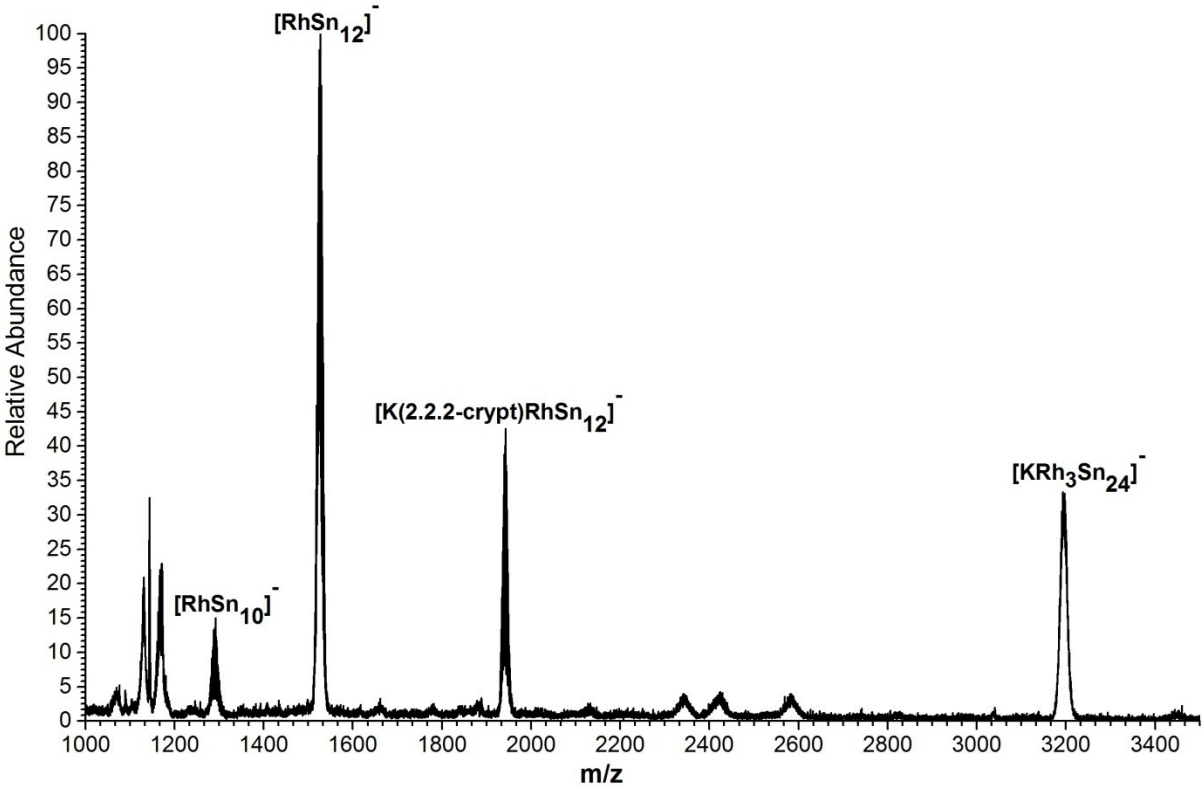

Figure S25. Overview ESI mass spectrum negative ion mode of the DMF reaction mixtures.

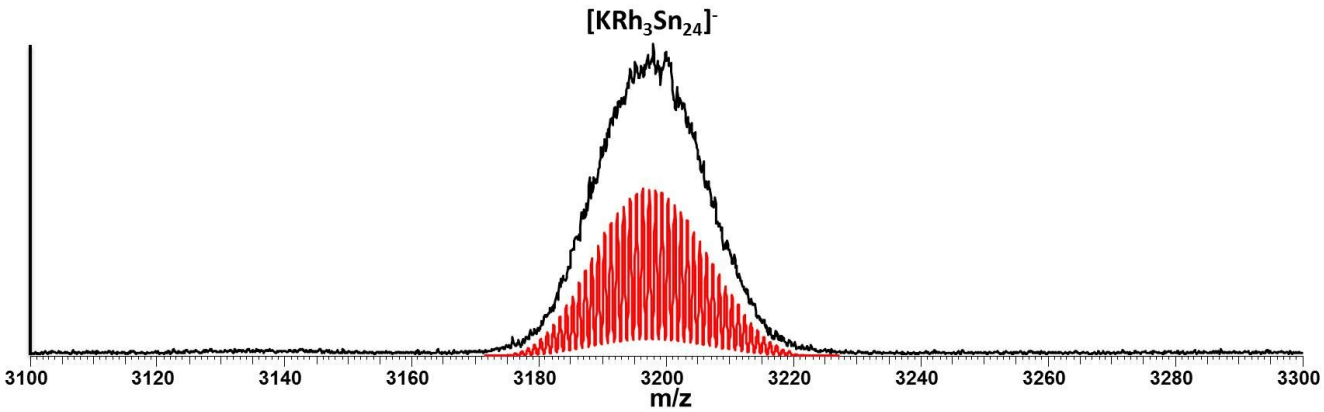

Figure S26. Measured (top) and simulated (bottom) spectrum of the fragment $[KRh_3Sn_{24}]^-$.

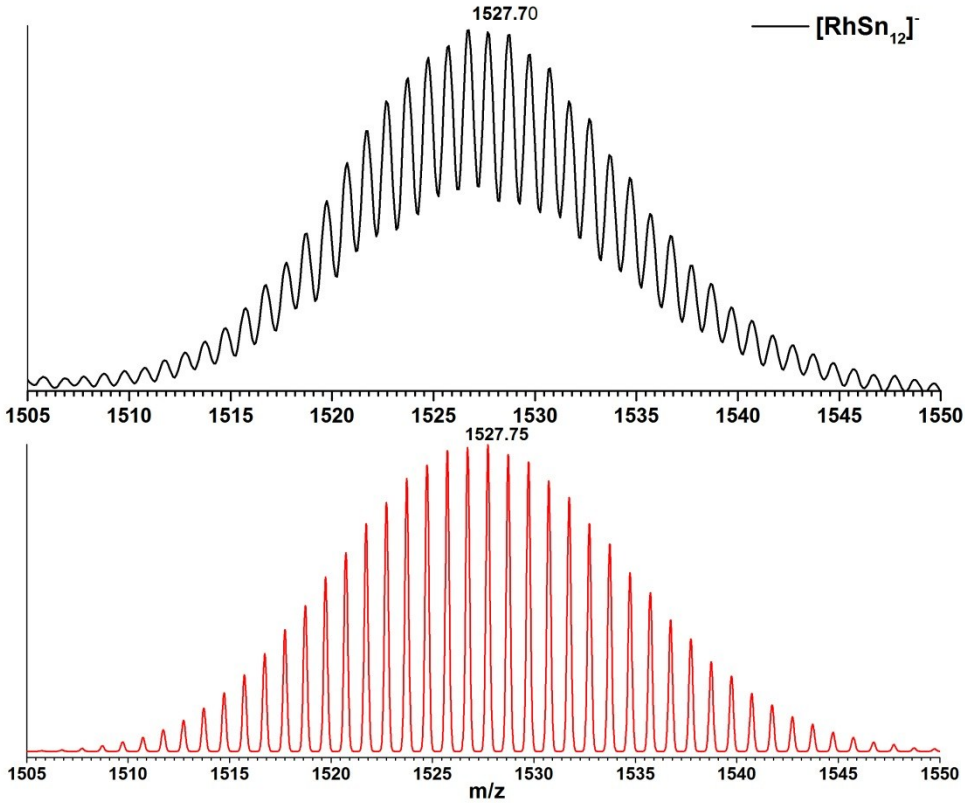

Figure S27. Measured (top) and simulated (bottom) spectrum of the fragment $[RhSn_{12}]^-$.

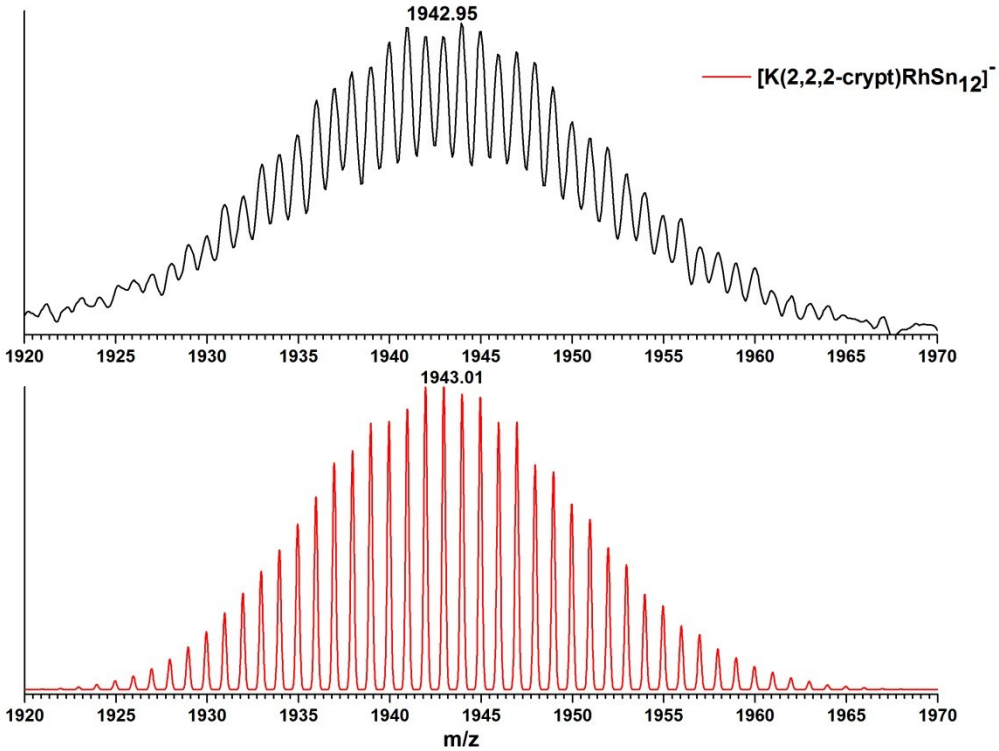

Figure S28. Measured (top) and simulated (bottom) spectrum of the fragment $[K(2,2,2\text{-crypt})RhSn_{12}]^-$.

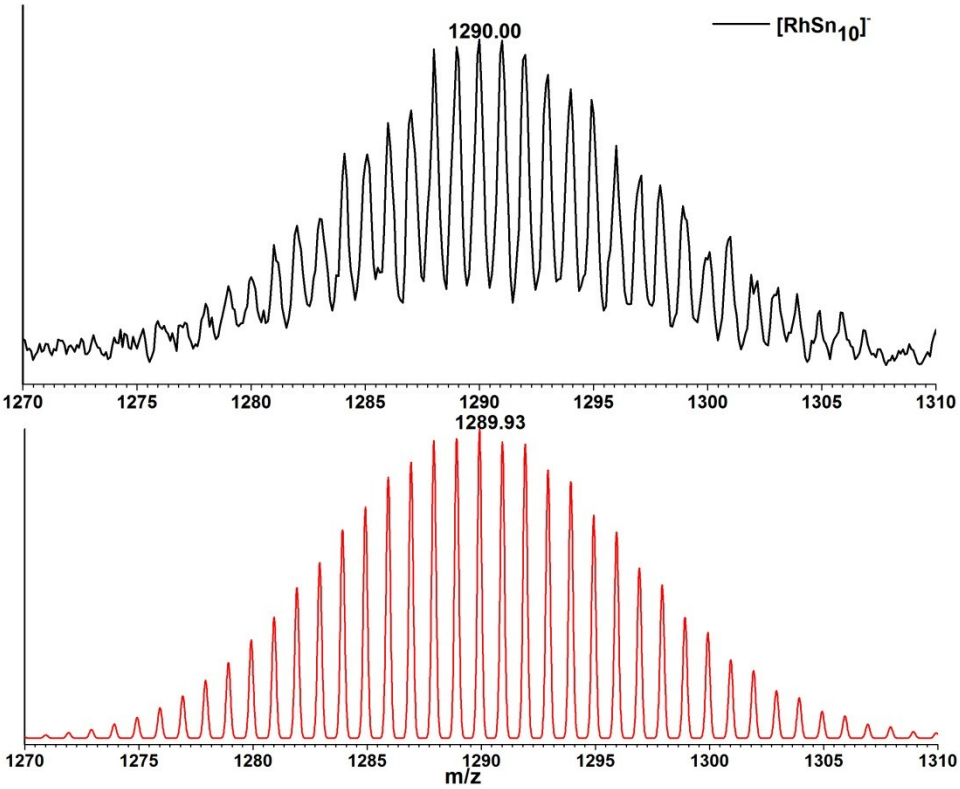

Figure S29. Measured (top) and simulated (bottom) spectrum of the fragment $[RhSn_{10}]^{-}$.

3.3 Detailed ESI mass spectrum of the single crystals of $[K(2,2,2\text{-crypt})]_3[Rh@Sn_{10}]$•en

The ESI-MS of the solution of the dissolved crystalline sample of $[K(2,2,2\text{-crypt})]_3[Rh@Sn_{10}]$•en in DMF shown in Figure 30 reveals a complex reaction mixture containing, in addition to $[Rh@Sn_{10}]^{1-}$ (m/z = 1289.92) and $\{K(2,2,2\text{-crypt})[Rh@Sn_{10}]\}^{1-}$ (m/z = 1705.17), prominent peaks at m/z = 1052.17 and 1091.08 due to $[Rh@Sn_8]^{1-}$ and $\{K[Rh@Sn_8]\}^{1-}$, respectively. Measured and simulated isotope distributions for all four species are shown in the supporting information, Figures S31-34.

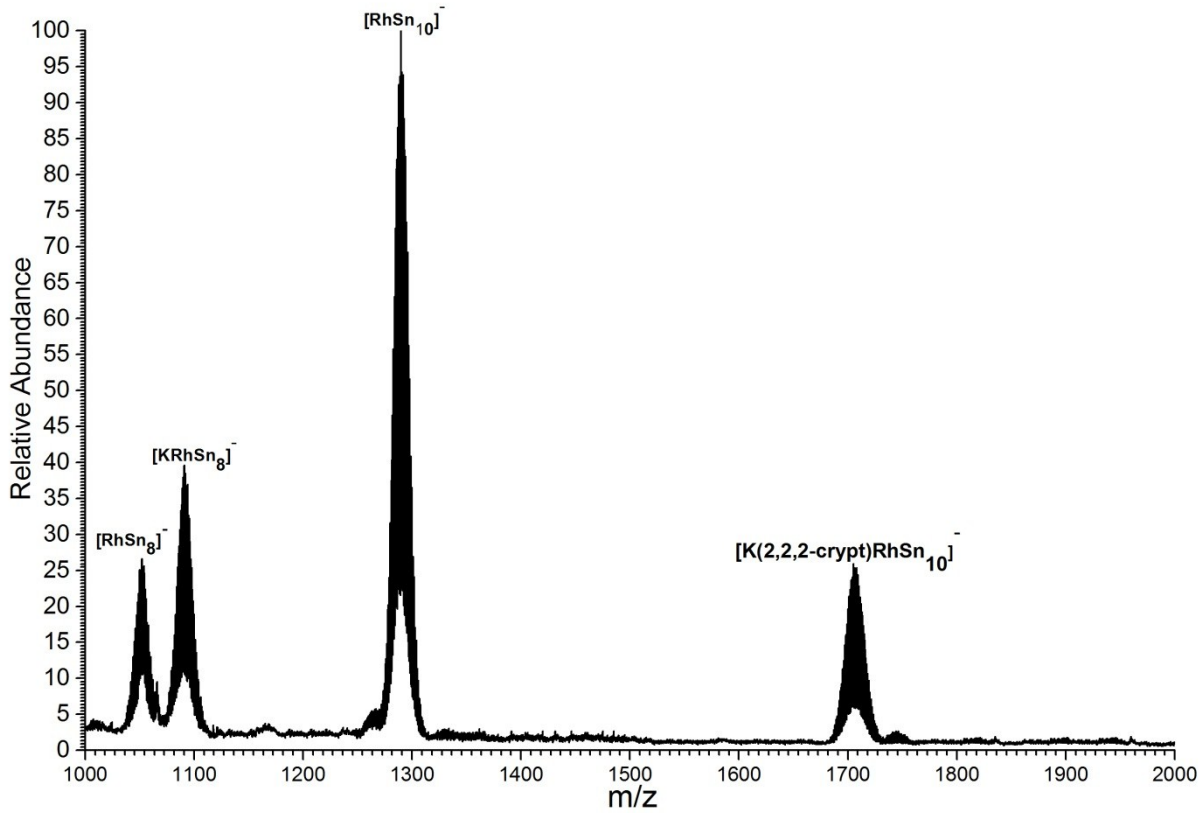

Figure 30. Overview ESI mass spectrum in negative ion mode of a freshly dissolved crystalline sample of $[K(2,2,2\text{-crypt})]_3[Rh@Sn_{10}]$•en in DMF.

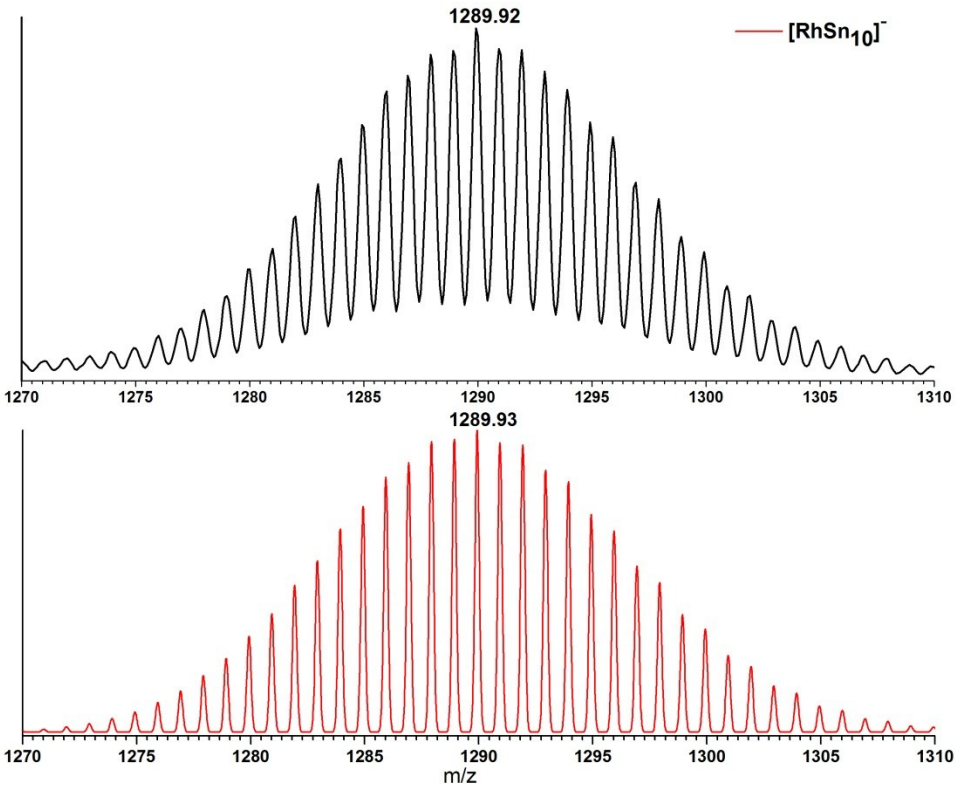

Figure S31. Measured (top) and simulated (bottom) spectrum of the fragment $[RhSn_{10}]^-$.

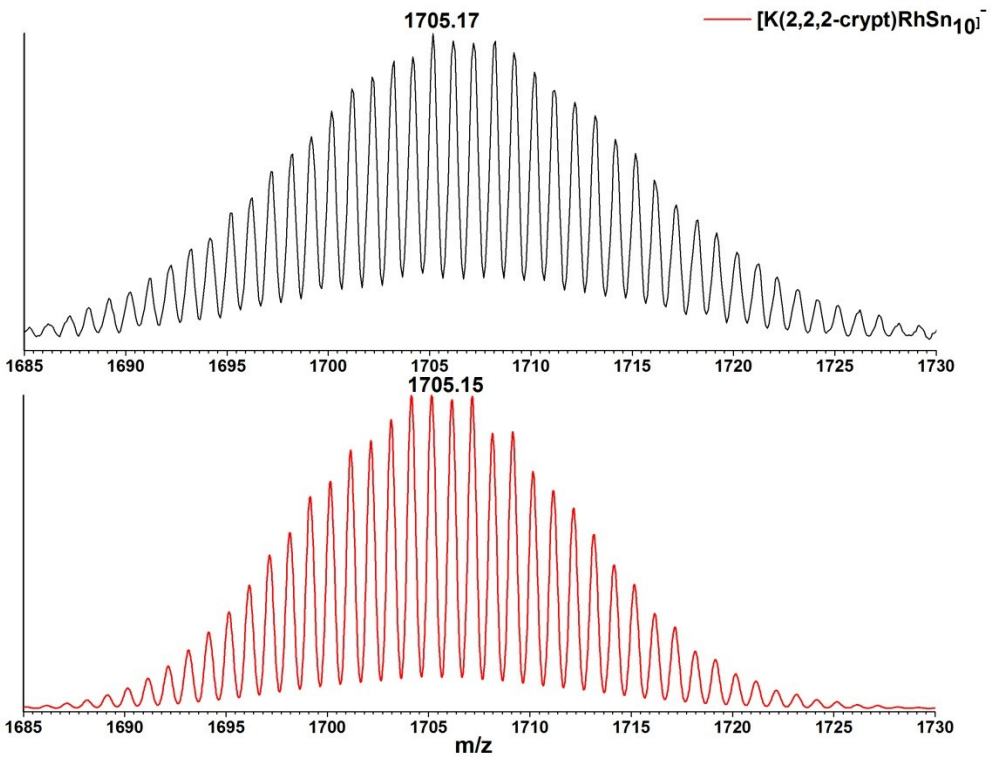

Figure S32. Measured (top) and simulated (bottom) spectrum of the fragment [K(2,2,2-crypt)RhSn$_{10}$] $^{-}$.

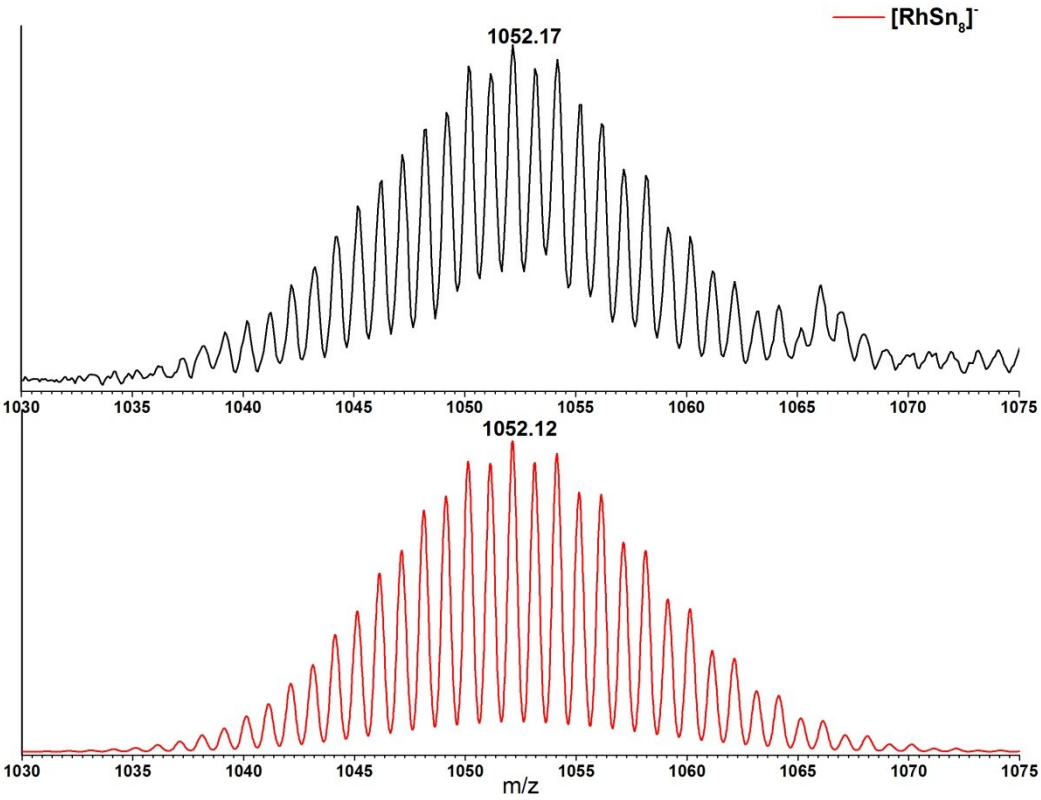

Figure S33. Measured (top) and simulated (bottom) spectrum of the fragment [RhSn$_{8}$] $^{-}$.

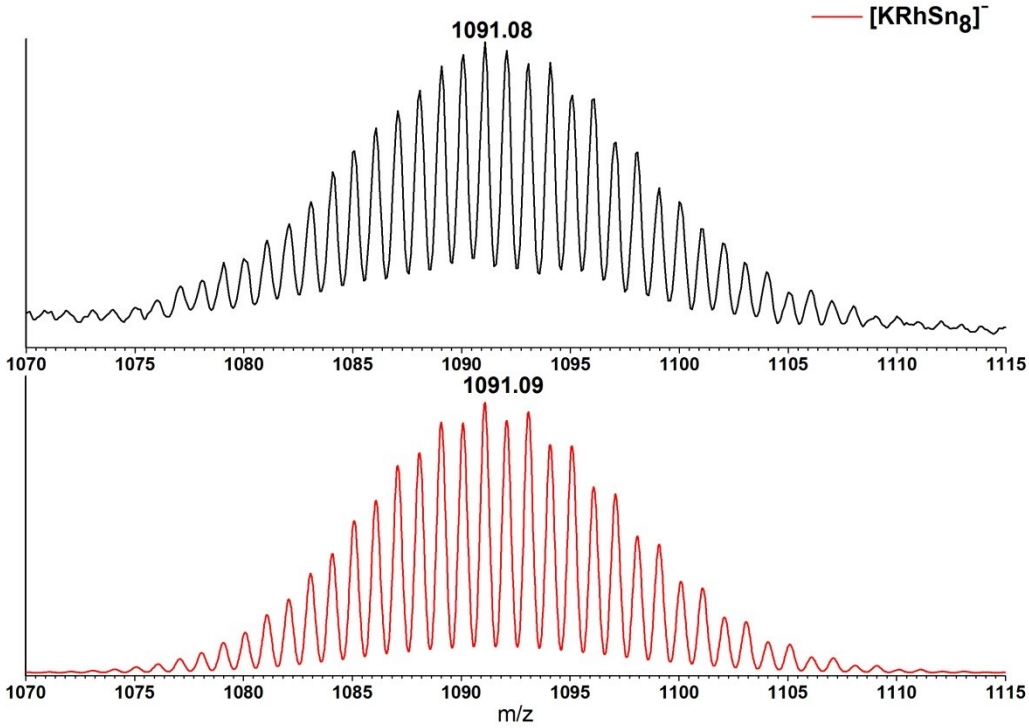

Figure S34. Measured (top) and simulated (bottom) spectrum of the fragment $[KRhSn_8]^-$.

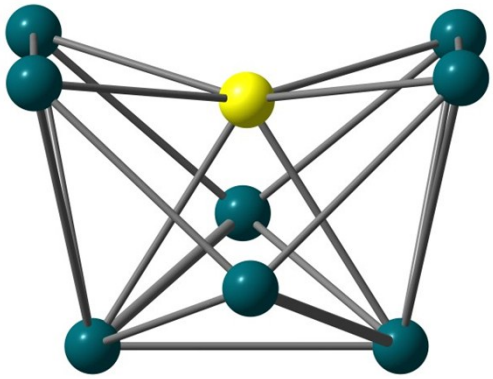

Figure S35. The DFT-optimized structure of the $[Rh@Sn_8]^-$ anion**.**

3.3 Detailed ESI mass spectrum of the single crystals of $[K(2,2,2\text{-crypt})]_3[Rh@Sn_{12}]\bullet 2Tol$

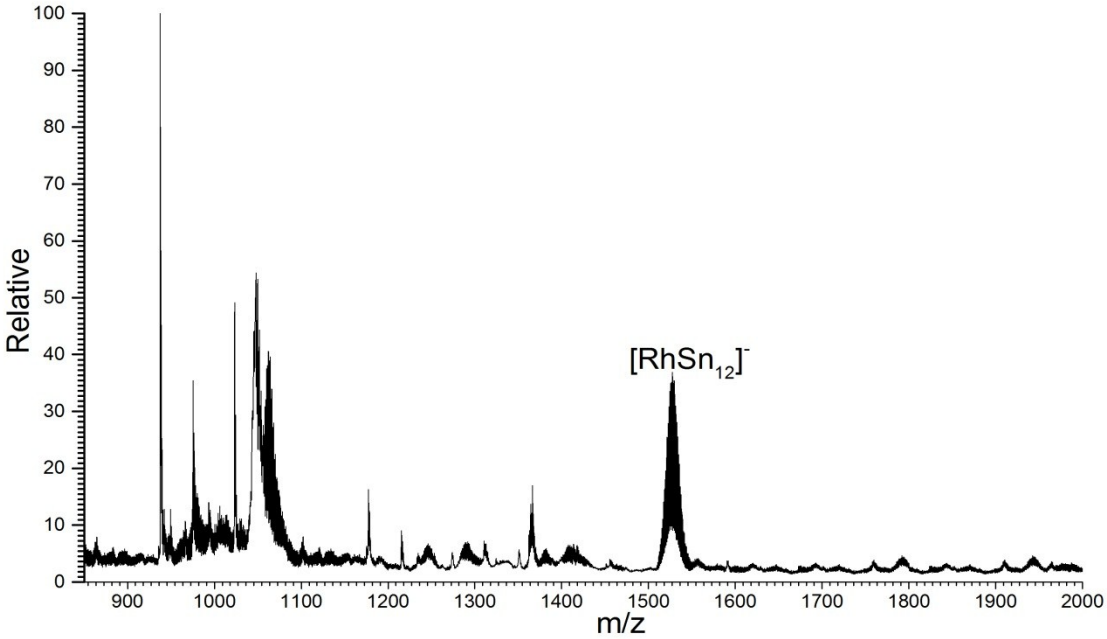

Figure S36. Negative ion mode ESI-MS of freshly dissolved crystals of $[K(2,2,2\text{-crypt})]_3[Rh@Sn_{12}]\bullet 2Tol$ in DMF.

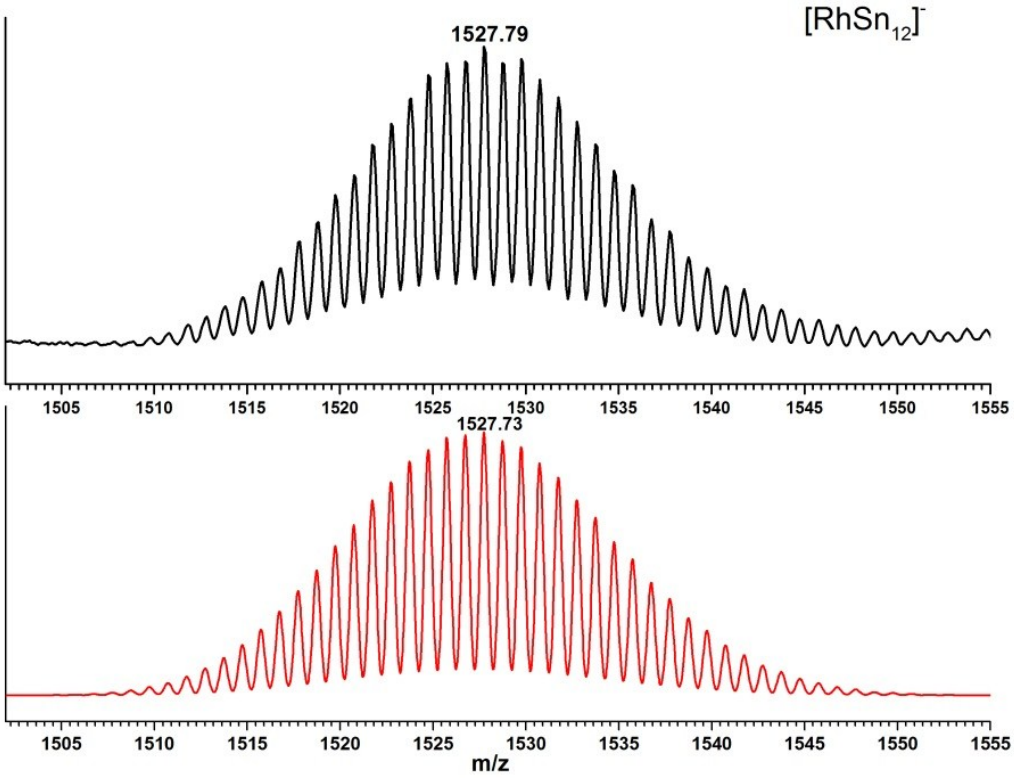

Figure S37. Measured (top) and simulated (bottom) spectrum of the fragment $[RhSn_{12}]^-$.

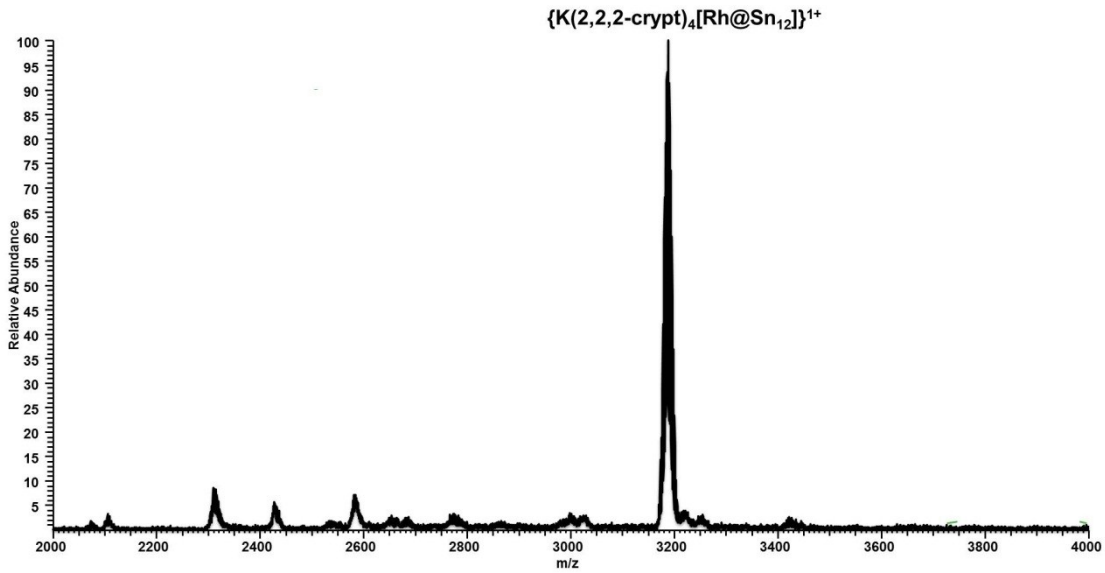

Figure S38. Positive ion mode ESI-MS of freshly dissolved crystals of $[K(2,2,2\text{-crypt})]_3[Rh@Sn_{12}]$•2Tol in DMF.

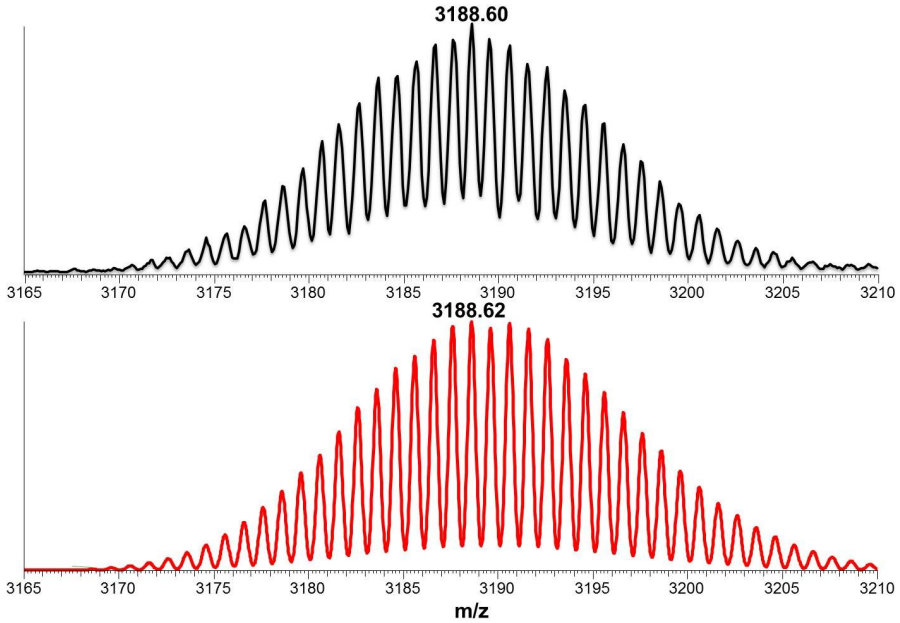

Figure S39. Measured (top) and simulated (bottom) spectrum of the fragment $\{K(2,2,2\text{-crypt})_4[RhSn_{12}]\}^+$.

3.4 Detailed ESI mass spectrum of the single crystals of $\{K_3[K(2,2,2\text{-crypt})]_3[Rh_2@Sn_{17}]\}$•4en

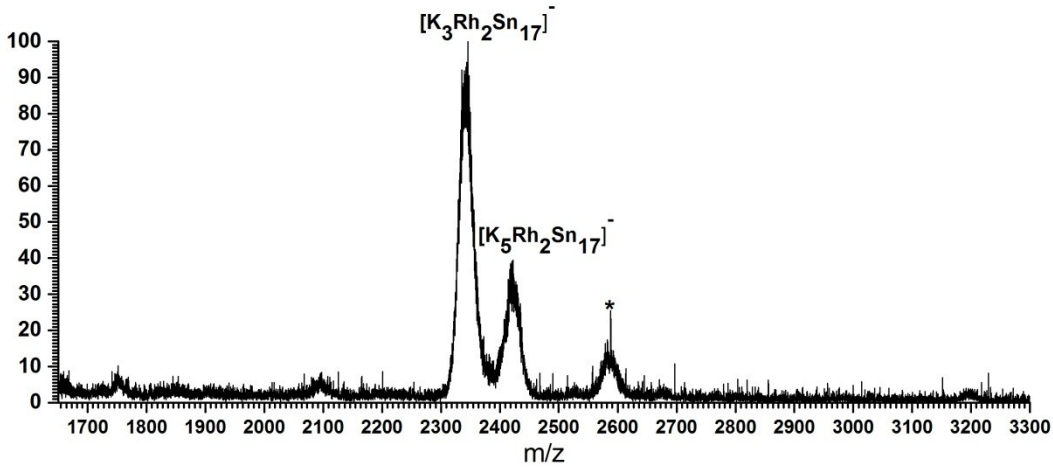

Figure S40. Negative-mode ESI-MS of the DMF solution of crystals of $\{K_3[K(2,2,2\text{-crypt})]_3[Rh_2@Sn_{17}]\}\bullet 4en$. Theoretical isotope distribution in red.

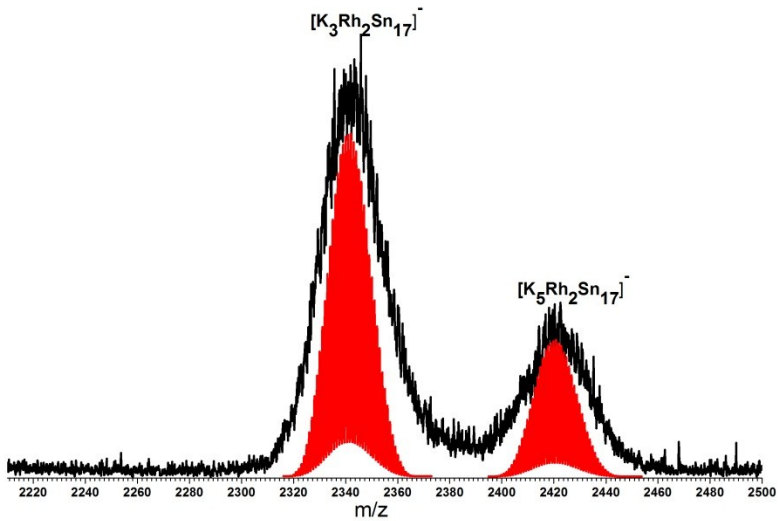

Figure S41. Measured and simulated spectrum of the fragments $[K_3Rh_2Sn_{17}]^-$ and $[K_5Rh_2Sn_{17}]^-$. Theoretical isotope distribution in red.

4. ^{119}Sn NMR Experiments.

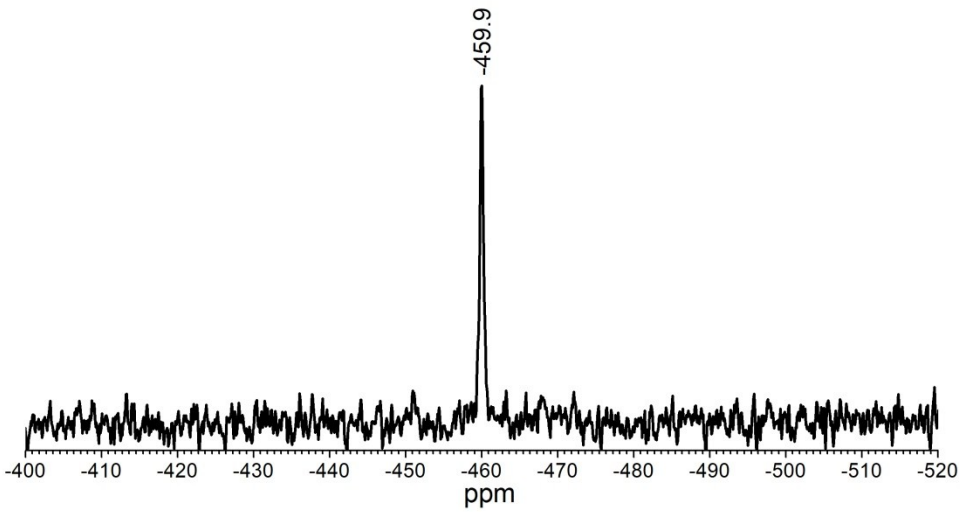

Figure S42. ^{119}Sn NMR spectrum of [K(2,2,2-crypt)]$_3$[Rh@Sn$_{12}$]•2Tol in e**n.**

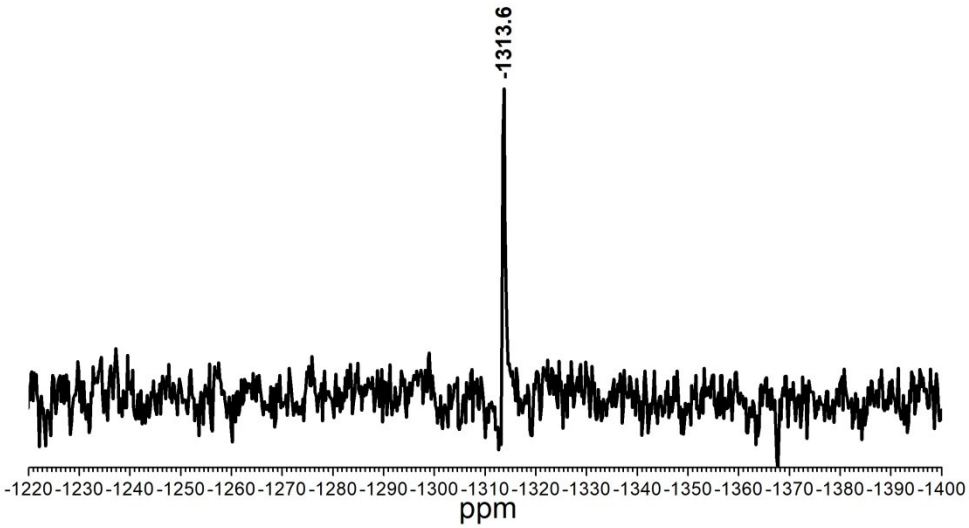

Figure S43. ^{119}Sn NMR spectrum **of** [K(2,2,2-crypt)]$_3$[Rh@Sn$_{10}$]•en in **e**n.

5. Energy Dispersive X-ray (EDX) Spectroscopic

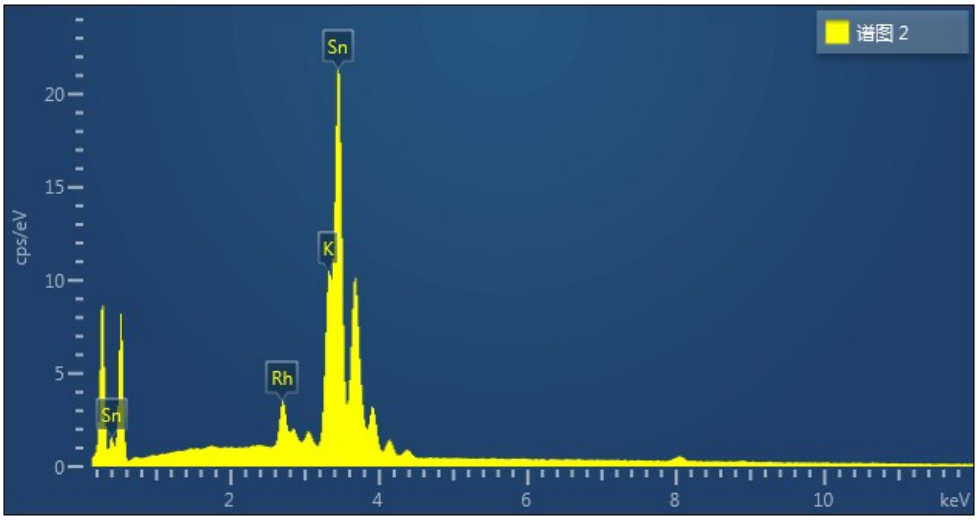

Elements	Series	wt%	wt% Sigma	Experimental / Calculated Atom %
K	K- Series	8.59	0.12	22.01/21.42
Rh	L- Series	6.53	0.15	6.36/7.14
Sn	L- Series	84.87	0.18	71.63/71.428
Total:		100.00		100.00

Figure S44. EDX analysis of [K([2.2.2]crypt)]$_3$[Rh@Sn$_{10}$]•en

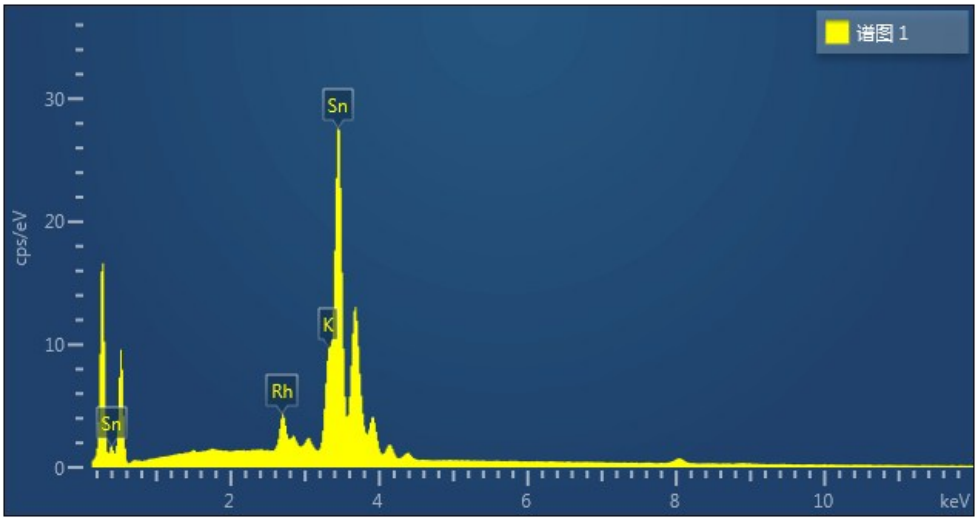

Elements	Series	wt%	wt% Sigma	Experimental / Calculated Atom %
K	K- Series	8.11	0.14	20.95/18.75
Rh	L- Series	6.26	0.16	6.15/6.25
Sn	L- Series	85.63	0.20	72.90/75
Total:		100.00		100.00

Figure S45. EDX analysis of $[K(2,2,2\text{-crypt})]_3[Rh@Sn_{12}]$•Tol

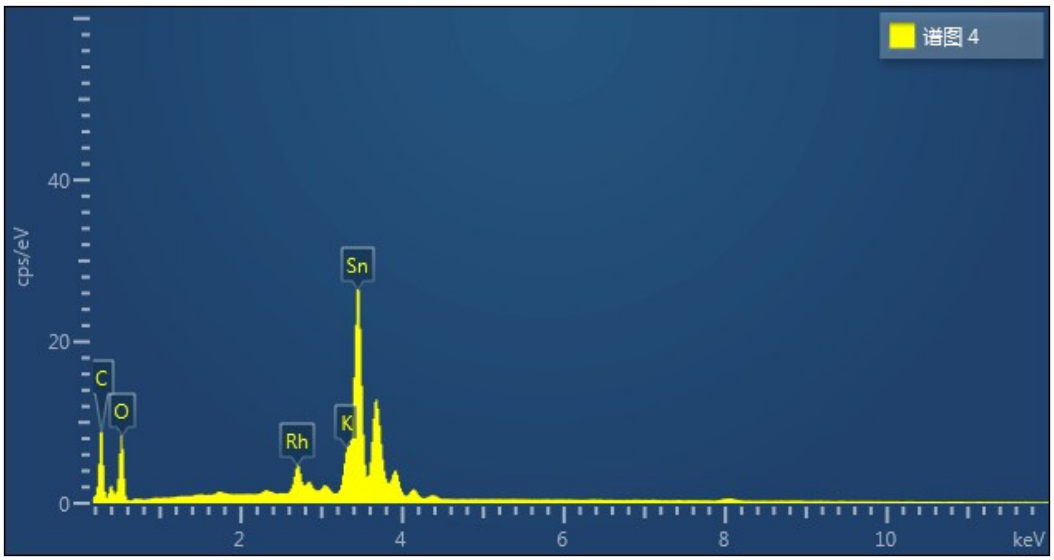

Elements	Series	wt%	wt% Sigma	Experimental / Calculated Atom %
K	K-Series	9.55	0.12	24.04/24
Rh	L-Series	7.61	0.16	7.28/8.00
Sn	L-Series	82.84	0.20	68.68/68
Total:		100.00		100.00

Figure S46. EDX analysis of $\{K_3[K(2,2,2\text{-crypt})]_3[Rh_2@Sn_{17}]$•4en.

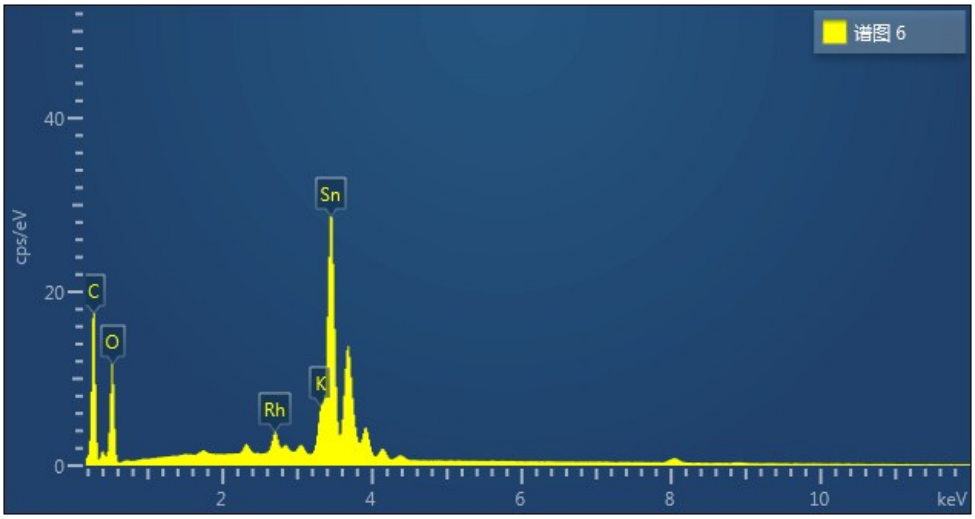

Elements	Series	wt%	wt% Sigma	Experimental / Calculated Atom %
K	K-Series	6.41	0.12	17.01/15.62
Rh	L-Series	9.29	0.15	9.36/9.375
Sn	L-Series	84.30	0.18	73.63/75
Total:		100.00		100.00

Figure S47. EDX analysis of $[K([2.2.2]crypt)]_5[Rh_3@Sn_{24}]$•2DMF•Tol.

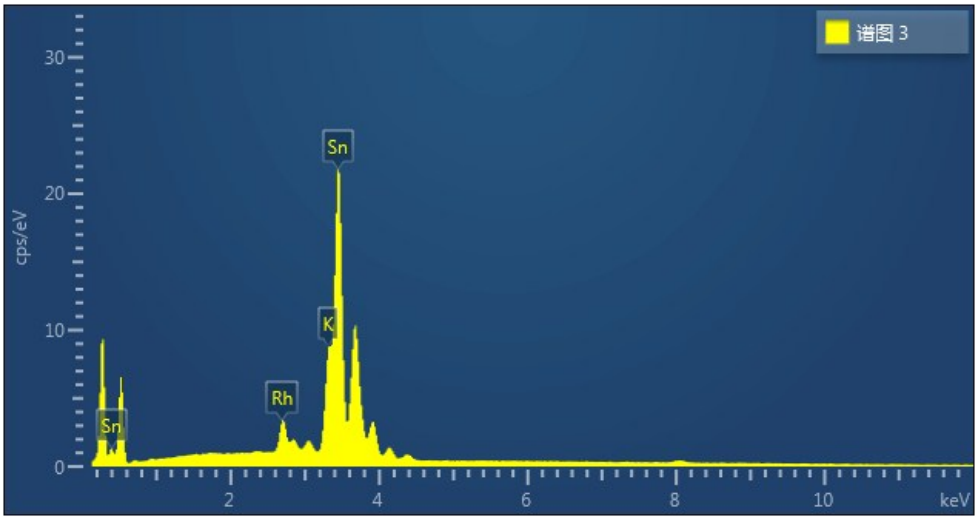

Elements	Series	wt%	wt% Sigma	Experimental / Calculated Atom %
K	K-Series	8.07	0.10	20.85/18.75
Rh	L-Series	6.67	0.14	6.55/6.25
Sn	L-Series	85.26	0.18	72.60/75
Total:		100.00		100.00

Figure S48. EDX analysis of $[K(2,2,2\text{-crypt})]_3[Rh@Sn_{12}]$•2DMF.

6. Total Energies and Optimised Coordinates of all DFT-computed Structures.

$[RhSn_{12}]^{3-}$: I_h symmetry. Total Energy -58.33022401 eV

Sn	1.572814	-2.164793	-1.338420
Sn	0.000000	-2.675832	1.338420
Rh	0.000000	0.000000	0.000000

Sn	-1.572814	-2.164793	-1.338420
Sn	-2.544867	0.826877	-1.338420
Sn	0.000000	0.000000	-2.991915
Sn	2.544867	0.826877	-1.338420
Sn	-1.572814	2.164793	1.338420
Sn	0.000000	2.675832	-1.338420
Sn	1.572814	2.164793	1.338420
Sn	2.544867	-0.826877	1.338420
Sn	0.000000	0.000000	2.991915
Sn	-2.544867	-0.826877	1.338420

$[RhSn_{10}]^{3-}$: C_{2v} symmetry. Total Energy -51.27572958 eV

Rh	0.000000	0.000000	0.075564
Sn	2.570573	0.000000	-1.083718
Sn	0.000000	-1.546729	-2.218523
Sn	1.702396	0.000000	2.234275
Sn	1.561715	2.405227	0.519388
Sn	1.561715	-2.405227	0.519388
Sn	0.000000	1.546729	-2.218523
Sn	-2.570573	0.000000	-1.083718
Sn	-1.561715	-2.405227	0.519388
Sn	-1.561715	2.405227	0.519388
Sn	-1.702396	0.000000	2.234275

$[RhSn_{10}]^{3-}$: D_{4d} symmetry. Total Energy -51.12078380 eV

Rh	0.000000	0.000000	0.000000
Sn	-0.946435	-2.284897	-1.225366
Sn	-2.284897	-0.946435	1.225366
Sn	2.284897	-0.946435	-1.225366
Sn	0.000000	0.000000	-3.035844
Sn	0.946435	-2.284897	1.225366
Sn	-2.284897	0.946435	-1.225366
Sn	-0.946435	2.284897	1.225366
Sn	0.000000	0.000000	3.035844
Sn	0.946435	2.284897	-1.225366
Sn	2.284897	0.946435	1.225366

$[RhSn_{10}]^{3-}$: D_{5h} symmetry. Total Energy -50.83269803 eV

Rh	0.000000	0.000000	0.000000
Sn	0.763414	2.349547	-1.508536
Sn	0.763414	2.349547	1.508536
Sn	-1.998644	1.452100	1.508536
Sn	2.470460	0.000000	1.508536
Sn	-1.998644	1.452100	-1.508536
Sn	2.470460	0.000000	-1.508536
Sn	-1.998644	-1.452100	1.508536
Sn	0.763414	-2.349547	1.508536
Sn	-1.998644	-1.452100	-1.508536
Sn	0.763414	-2.349547	-1.508536

$[Rh_2Sn_{17}]^{6-}$: D_{2d} symmetry. Total Energy -92.78558694 eV

Rh	0.000000	0.000000	-2.528312
Rh	0.000000	0.000000	2.528312
Sn	-2.656023	-0.498629	1.863334
Sn	2.656023	-0.498629	-1.863334
Sn	-1.766322	-1.766322	-3.780392
Sn	2.656023	0.498629	1.863334
Sn	1.137107	-1.137107	-4.768730
Sn	0.498629	2.656023	1.863334
Sn	-1.766322	1.766322	3.780392
Sn	-1.137107	-1.137107	4.768730
Sn	1.137107	1.137107	4.768730
Sn	1.766322	1.766322	-3.780392
Sn	-2.656023	0.498629	-1.863334
Sn	0.000000	0.000000	0.000000
Sn	-1.137107	1.137107	-4.768730
Sn	-0.498629	-2.656023	1.863334

Sn	1.766322	-1.766322	3.780392
Sn	0.498629	-2.656023	-1.863334
Sn	-0.498629	2.656023	-1.863334

$[K_3Rh_2Sn_{17}]^{3-}$: C_s symmetry. Total Energy -89.66356263 eV

Rh	2.510214	-0.374714	0.000000
Sn	-1.923739	-2.015088	-1.501661
Sn	2.243314	1.154493	2.300111
Sn	3.363379	-3.055586	0.000000
Sn	-1.847488	2.477148	1.540113
Sn	4.751020	-0.744230	1.603145
Sn	-1.847488	2.477148	-1.540113
Sn	-3.818461	0.292013	-2.475390
Sn	-4.841897	-1.222312	0.000000
Sn	-4.660899	2.015423	0.000000
Sn	4.247301	1.855022	0.000000
Sn	1.558663	-1.836467	-2.146596
Sn	0.048723	0.269592	0.000000
Rh	-2.494861	0.250322	0.000000
Sn	4.751020	-0.744230	-1.603145
Sn	-1.923739	-2.015088	1.501661
Sn	-3.818461	0.292013	2.475390
Sn	1.558663	-1.836467	2.146596
Sn	2.243314	1.154493	-2.300111
K	1.217039	4.078645	0.000000
K	-0.627227	0.187414	4.408260
K	-0.627227	0.187414	-4.408260

$[Rh_3Sn_{24}]^{5-}$: C_{3v} symmetry. Total Energy -121.35709311 eV

Sn	-0.909824	1.575862	-1.822725
Sn	-3.874439	1.524290	2.204801
Sn	-5.529074	0.000000	0.047388
Sn	-3.812927	-2.498505	-0.702649
Sn	-3.812927	2.498505	-0.702649
Sn	-0.910827	-1.577599	1.386635
Sn	-0.910827	1.577599	1.386635
Sn	-0.909824	-1.575862	-1.822725
Sn	-3.852660	0.000000	-2.562628
Sn	1.819649	0.000000	-1.822725
Sn	-0.257305	4.551344	-0.702649
Sn	-3.874439	-1.524290	2.204801
Sn	1.821654	0.000000	1.386635
Sn	0.617146	-4.117508	2.204801
Sn	0.617146	4.117508	2.204801
Sn	-0.257305	-4.551344	-0.702649
Sn	1.926330	-3.336502	-2.562628
Sn	4.070232	2.052839	-0.702649
Sn	4.070232	-2.052839	-0.702649
Sn	1.926330	3.336502	-2.562628
Sn	2.764537	4.788319	0.047388
Sn	2.764537	-4.788319	0.047388
Sn	3.257293	2.593218	2.204801
Sn	3.257293	-2.593218	2.204801
Rh	-2.640943	0.000000	-0.058780
Rh	1.320471	-2.287123	-0.058780
Rh	1.320471	2.287123	-0.058780

7. References

[1] A. Vanderent, A. L, Onderdelinden, *Inorg. Synth*. **1973,** *14*, 93-95

[2] a) O. V. Dolomanov, L. J. Bourhis, R. J. Gildea, J. A. K. Howard, H. Puschmann, *J. Appl. Crystallogr*. **2009**, *42*, 339. b) G. M. Sheldrick, ShelXL2014; University of Göttingen: Göttingen, Germany.

[3] A. L. Spek,. Structure validation in chemical crystallography. *Acta Crystallogr., Sect. D: Biol. Crystallogr*. **2009**, *65*, 148−155.

[4] ADF2017, , E. J. Baerends, *et al*., SCM, Theoretical Chemistry, Vrije Universiteit, Amsterdam, The Netherlands, http://www.scm.com, 2017.

[5] G. te Velde, F. M. Bickelhaupt, E. J. Baerends, C. Fonseca Guerra, S. J. A. van Gisbergen, J. G. Snijders, T. Ziegler, *J. Comput. Chem*., **2001**, *22*, 931-967.

[6] C. Fonseca Guerra, G. J. Snijders,; G. te Velde, E. J. Baerends, *Theor. Chem. Acc*., **1998**, *99*, 391-403.

[7] A. D. Becke, *Phys. Rev. A*, **1988**, *38*, 3098.

[8] J. P. Perdew, *Phys. Rev. B: Condens. Matter*, **1986**, *33*, 8822.
[9] E. van Lenthe, E. J. Baerends, *J Comput Chem*., **2003**, *24*, 1142-1156.
[10] E. van Lenthe, E. J.Baerends, J. G.Snijders, *J. Chem. Phys*., **1994**, *101*, 9783-9702
[11] L. Versluis, T. Ziegler, *J. Chem. Phys.*, **1988**, *88*, 322-328.
[12] C. C. Pye, T. Ziegler, *Theor. Chem. Acc.*, **1999***, 101*, 396-408.
[13] He, H. "*Synthesis and Characterization of Tin Polyanions Endohedrally Filled with Transition Metal Group 9 Atoms*", PhD Thesis, Technische Universität München, **2014**.
[14] P. Murray-Rust, H. B..Bürgi, J. D. Dunitz, *J. Am. Chem. Soc*., **1975**, *97*, 921.
[15] L. Bartell, *J. Chem. Phys*. **1967**, *46*, 4530.
[16] M. Kaupp, Ch. Van Wüllen, R. Franke, F. Schmitz, W. Kutzelnigg, *J. Am. Chem. Soc*., **1996**, *118*, 11939-11950.